SOME PHYSICAL AND MAGNETIC PROPERTIES OF DC SPUTTERED Bi(Pb)SrCaCuO THIN FILM

by

SEVGİ BAL

THESIS SUBMITTED TO

THE GRADUATE SCHOOL OF NATURAL AND APPLIED SCIENCES

OF

THE ABANT İZZET BAYSAL UNIVERSITY

IN PARTIAL FULFILLMENT OF THE REQUIREMENTS FOR THE DEGREE

OF

MASTER OF SCIENCE

IN

THE DEPARTMENT OF PHYSICS

JUNE 2011

Approval of the Graduate School of Natural and Applied Science

Prof. Dr. Nihat ÇELEBİ
Director

I certify that this thesis satisfies all the requirements as a thesis for the degree of Master of Science.

Prof. Dr. Kıvılcım KILIÇ
Head of Physics Department

This is to certify that we have read this thesis and that in our opinion it is fully adequate, in scope and quality as a thesis for the degree of Master of Science.

Prof. Dr. Ahmet VARİLCİ
Supervisor

Examining Committee Members:

1. Prof. Dr. Ahmet VARİLCİ …….
2. Assoc. Prof. Dr. Cabir TERZİOĞLU …….
3. Assist. Prof. Dr. Erhan BUDAK …….

ABSTRACT

SOME PHYSICAL AND MAGNETIC PROPERTIES OF DC SPUTTERED Bi(Pb)SrCaCuO THIN FILM

BAL, Sevgi

Master of Science, Department of Physics

Supervisor: Prof. Dr. Ahmet VARİLCİ

June 2011, 84 Pages

In this thesis, the most suitable annealing condition for the Bi(Pb)SrCaCuO (Bi-2212) thin films produced by standard direct current (DC) magnetron reactive sputtering method at 100 watt on the magnesium oxide (MgO) single crystal substrate was investigated. Moreover, some physical and magnetic properties of the thin films annealed at 840^0C and 850^0C for different annealing times (1h, 2h, 4h, 6h and 8h) were examined. DC sputter device, cryostat system, X-ray diffractometer (XRD), scanning electron microscopy (SEM) and energy dispersive spectrum analysis were used to obtain the experimental results. At first, target of the thin film samples produced in this work was prepared by means of

solid state reaction method. Ten Bi(Pb)SrCaCuO (Bi-2212) thin films were produced on the magnesium oxide at DC sputter device. The effect of different annealing times on the superconducting critical temperature (T_c) of Bi(Pb)SrCaCuO thin films was investigated by the resistivity measurements. These measurements were performed by helium gas contact cryostat in the temperature range from 30 to 120 K with DC current of 1 mA. Moreover, resistivity dependence of temperature measurements for only the film annealed at 840^0C for 2 hours were carried out under field strengths of 0, 0.5, 1, 3 and 5 T, which were parallel and perpendicular to the film surface. X-ray diffraction graphs were obtained and the peaks on these graphs were determined by the help of the literature. Volume fractions of Bi-2223 and Bi-2212 and lattices parameters of the all films were also calculated. After that, the images of scanning electron microscopy were obtained to analyze the surface morphology. Finally, the results of energy dispersive spectrum analysis of the Bi(Pb)SrCaCuO thin films were also taken and the weight percent of elements of these films were theoretically calculated.

KEY WORDS: Bi-2223, Bi-2212, High temperature superconductors, Transition temperature, Mechanical properties.

ÖZET

DOĞRU AKIM PÜSKÜRTME YÖNTEMİ İLE ÜRETİLMİŞ Bi(Pb)SrCaCuO İNCE FİLMLERİN BAZI FİZİKSEL VE MANYETİK ÖZELLİKLERİ

BAL, Sevgi

Yüksek Lisans, Fizik Bölümü

Tez Danışmanı: Prof. Dr. Ahmet VARİLCİ

Haziran 2011, 84 Sayfa

Bu tezde, tek kristal yapıya sahip olan magnezyum oksit üzerine 100 Watt'da standart doğru akım (DC) reaktif püskürtme yöntemi ile üretilen Bi(Pb)SrCaCuO (Bi-2212) ince filmler için en uygun tavlama koşulları araştırıldı. Ayrıca, 840^0C ve 850^0C' de değişik tavlama sürelerinde (1sa, 2sa, 4sa, 6sa and 8sa) tavlanan ince filmlerin bazı fiziksel ve manyetik özellikleri incelendi. Deneysel verileri elde etmek için DC püskürtme cihazı, kriyostat sistemi, X-ışınları kırınım (XRD) cihazı, taramalı elektron mikroskopu (SEM) ve enerji dağılımı spektrum analizi (EDS) kullanıldı. İlk olarak bu çalışmada üretilen ince

filmlerin hedef malzemesi katıhal tepkime yöntemiyle hazırlandı. Doğru akım püskürtme cihazında on adet Bi(Pb)SrCaCuO (Bi-2212) ince film magnezyum oksit üzerine üretildi. Özdirenç ölçümleri ile değişik tavlama sürelerinin Bi(Pb)SrCaCuO ince filmlerin süperiletken kritik sıcaklığı (T_c) üzerine etkisi incelendi. Bu ölçümler 30 ile 120 K sıcaklığı aralığında 1 mA' lik doğru akım altında helyum gaz bağlantılı kriyostat tarafından yapıldı. Ayrıca film yüzeyine paralel ve dik olarak uygulanan 0, 0.5, 1, 3 and 5 T'lık manyetik alan kuvvetleri altında sadece 840^0C'de 2 saat tavlanan film için sıcaklığa bağlı özdirenç ölçümleri yapıldı. X-ışınları kırınım grafikleri elde edildi ve bu grafiklerin üzerindeki zirve noktaları literatür yardımı ile belirlendi. Ayrıca Bi-2212 ve Bi-2223 hacim oranları ve kafes parametreleri hesaplandı. Sonra yüzey morfolojisini incelemek için taramalı elektron mikroskobu görüntüleri alındı. Son olarak da Bi(Pb)SrCaCuO ince filmlerin enerji dağılımı spektrum analizleri alındı ve elementlerin yüzde ağırlığı hesaplandı.

ANAHTAR KELİMELER: Bi-2212, Bi-2223, Yüksek sıcaklık süperiletkenler, Geçiş sıcaklığı, Mekanik Özellikler.

TO MY PARENTS…

ACKNOWLEDGEMENT

It is a great pleasure to thank many people who have contributed to the completion of this thesis.

First of all, I would like to thank my thesis supervisor, Prof. Dr. Ahmet Varilci for his guidance, support, encouragement and patience during the preparation of this thesis. He taught not only a great deal of major viewpoints about physics but also to be a decisive and patient researcher.

I thank to Assoc. Prof. Dr. Cabir Terzioğlu for many discussions and enlightening comments on my works.

I also acknowledge to Assoc. Prof. Dr. Cabir Terzioğlu again and Asist. Prof. Dr. Erhan Budak along with my advisor for serving on my thesis committee.

I am grateful to Assist. Prof. Dr. Mustafa Akdoğan and R. A. Gürcan Yıldırım for their effort, kind help and support during the preparation of sample and carrying out experimental measurements.

At last, I want to thank my family for their continuous support, patience and encouragement which made it possible for me to keep on my study.

TABLE OF CONTENTS

Page

LIST OF TABLES

TABLE **Page**

LIST OF FIGURES

FIGURE **Page**

CHAPTER 1

INTRODUCTION

1.1 HISTORY OF SUPERCONDUCTIVITY

At first, H. Kamerlingh-Onnes discovered the phenomenon of superconductivity in 1911. He measured the resistance of mercury at very low temperatures. Onnes wanted to find out how small the resistance to an electric current can be obtained if a substance is purified and the temperature (thermal noise) is lowered as much as possible. However, they observed that the resistance disappeared almost instantaneously at a temperature below 4.15 K. Figure 1.1 represents the behavior of resistance as a function of temperature schematically **[1]**.

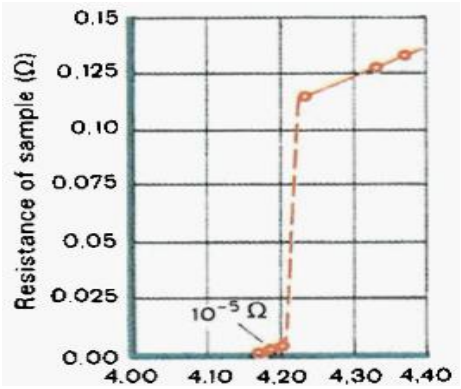

Figure 1.1: Data from one of Onnes' pioneering works devoted to superconductivity. According to current data , the curve should now be shifted by 0.05 K, since the temperature scale used by Onnes was inaccurate **[1]**.

The next development is understanding how matter acts at so cold temperatures occurred in 1933 by German scientists Walther Meissner and Robert Ochsenfeld. They found that a superconducting material will repel a magnetic field. A magnet which is moving by a conductor induces currents in the conductor. This is the rule on which the electric generator operates. However, in a superconductor the induced currents exactly mirror the field that would have otherwise penetrated the superconducting material-causing the magnet to be repulsed. This phenomenon is known as strong diamagnetism. Today, it is often referred to as the Meissner Effect. That effect is so strong that a magnet can actually be levitated over a superconductive material.

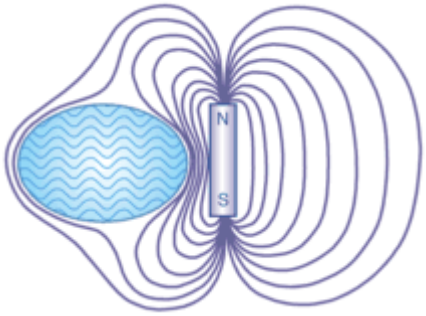

Figure 1.2: Meissner Effect.

In following decades other superconducting metals, alloys and compounds were discovered. Niobium-nitride was found to superconductor at 16 K in 1941. Then, vanadium-silicon performed superconductive properties at 17.5 K in 1953. And, in 1962 scientists at Westinghouse were developed the first commercial superconducting wire with an alloy of niobium and titanium (NbTi). After that, high-energy, particle-accelerator electromagnets made of copper-clad niobium-titanium were improved in the 1960s at the Rutherford-Appleton Laboratory in

the UK. In 1987, they were firstly used in a superconducting accelerator in the US.

In 1950 Vitaly Ginzburg and Landau aimed an intuitive, phenomenological theory (often called ‘macroscopic theory’) of superconductivity. Their approach turned out to be surprisingly successful and, one can obtain useful insight into the characteristic properties of most interesting superconductor materials (including high T_c oxides) by applying the results of the Ginzburg-Landau theory. In 1957, Alexei Abrikosov studied the behaviour of superconductors in an external magnetic field and discovered that one can distinguish two types of material: type-I and type-II superconductors. While the former expel magnetic flux completely from their interior, the latter do it completely only at small fields, but partially in higher external fields. Thanks to this, i.e, the formation of the so-called mixed state, these materials can sustain superconductivity even in fields higher than10 Tesla. Type-II superconductors are therefore the ones that are of interest for most large scale applications **[2].**

American physicists John Bardeen, Leon Cooper, and John Schrieffer improved the first widely-accepted theoretical understanding of superconductivity in 1957. Their theories is known as the BCS theory. It is derived from the first letter of each man's last name. BCS theory is explained superconductivity at temperatures close to absolute zero for elements and alloys. But later, at higher temperatures and with different superconductor systems, the BCS theory has become inadequate to explain how superconductivity is occurring **[26].**

In 1962, an English physicist B. Josephson predicted theoretically some unusual phenomena that occurred on superconductor contacts. These predictions were then fully confirmed and the phenomenon itself was called weak

superconductivity or the Josephson effect, and soon found practical applications **[1].**

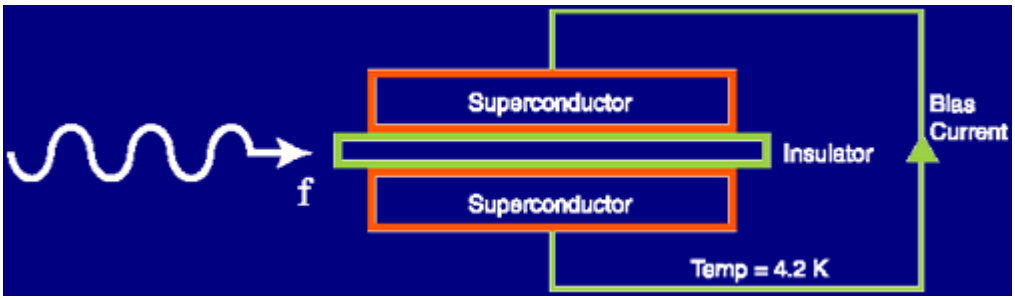

Figure 1.3: Schematic representation of a Josephson junction.

Bednorz and Müller discovered high temperature superconductivity in layered materials dominated by copper oxide planes in 1986. Materials of this sort have subsequently been discovered with T_c well over 100 K. This has opened the way to a broader range of practical applications than for the classic superconductors because cooling by liquid helium is not required. Realization of these applications has not been immediate, however, because these oxide materials are hard to fabricate in useful forms and have low electron densities compared to conventional metals. Resistance causing fluctuations are much more prominent than in the classic superconductors for several reasons: (1) operations at higher temperatures inevitably thermal fluctuations more important; (2) the higher T_c and low Fermi velocity stemming from the low electron density implies a short coherence length, which allows easier fluctuations; and (3) the anisotropy induced by the weak interplanar coupling reduces the integrity of vortex lines, so that pinning is less effective. Despite these practical obstacles, the intellectual challenge of understanding these unusual materials has motivated an enormous volume of research, and remarkable progress has been made **[3].**

In February 1987 research groups in Alabama and Houston, coordinated by K. Wu and Paul Chu discovered $Y_1Ba_2Cu_3O_7$ ceramics with T_c=92 . This was an important discovery as it meant that for the first time the world has witnessed the existence of a superconductor with a critical temperature above that of a liquid nitrogen which is a much cheaper coolant than liquid helium. It is very easy to prepare $Y_1Ba_2Cu_3O_7$ ceramics by mixing, calcining and oxidizing the constituent powders so that such experiments are being done even by high school students. Only a year later, early in 1988, Bi and Tl-cuprate oxides were discovered with T_c=110 and 125 K respectively. Since than, several research groups have claimed even higher transition temperatures, but none of them were reproducible or independently confirmed by other laboratories **[2].**

In 1997 researchers obtained that at a temperature very near absolute zero an alloy of gold and indium was both a superconductor and a natural magnet. Conventional wisdom held that a material with such properties could not exist. Then, over a half-dozen such compounds have been found. In 2000, it has also seen that the discovery of the first high-temperature superconductor does not contain any copper. Moreover, the first all-metal perovskite superconductor was found in 2001.

Also, in 2001 a material that had been sitting on laboratory shelves for decades was measured by Japanese researches. And, it was seen that that material is an extraordinary new superconductor. It is found that the transition temperature of magnesium diboride at 39 Kelvin - far above the highest T_c of any of the elemental or binary alloy superconductors. While 39 K is still well below the T_c's of the "warm" ceramic superconductors, subsequent refinements in the way MgB_2

is fabricated have paved the way for its use in industrial applications. Laboratory testing has found MgB_2 will outperform NbTi and Nb_3Sn wires in high magnetic field applications like MRI.

Finally, the discovery of high critical temperature iron and arsenic superconductors (AsFe) were found in 2008. That compounds do not contain copper (Cu) but have oxygen (O), flour (F) or arsenic (As) and iron (Fe). So, this improvement will help scientists to solve some of the mysteries in the area of solid state physics.

CHAPTER 2

PROPERTIES OF SUPERCONDUCTIVITY

2.1 INTRODUCTION

When electrical current flows, there is some resistance to the motion of electrons through the materials which are normal conductors for many materials. It is essential to apply a voltage to conserve the current flowing, to replace the energy dissipated by the resistance. For example, a copper wire in a house is a well enough conductor, with only a little resistance. The filament of a light bulb has a high resistance, and forms so much heat that light is given off. Electronics is stand on components in which the resistance changes under control of an input voltage; these components are compose of semiconductors. However, a superconductor has no resistance at all **[4].**

Superconductivity is an electrical resistance of certainly zero which occurs in some materials when they are cooled to extremely low temperatures **[2].**

2.2 SUPERCONDUCTING TRANSITION TEMPERATURE

Transition temperature is defined as the temperature at which a superconductor loss electrical resistance is called superconducting “transition temperature” or “critical temperature” written as $T_{c.}$ It is a characteristic property. Hence, it is different for each metal as shown in Table 2.1. The transition is so rapid and complete that appears to different phase of matter. Above a critical

temperature T_c, the properties of metal are completely normal. In other words, the superconducting properties are not displayed. However, below T_c. Superconducting properties are valid, the most dramatic of which is the absence of any measurable DC electrical resistance **[5].**

ELEMENTS	**T_c (K)**	**H_c (GAUSS)**
Al	1.196	99
Cd	0.56	30
Ga	1.091	51
Hf	0.09	--
Hg χ rhomb	4.15	411
β	3.95	339
In	3.40	293
Ir	0.14	19
La χ (hcp)	4.9	798
β (fcc)	6.06	1096
Mo	0.92	98
Nb	9.26	1980
Os	0.655	65
Pa	1.4	--
Pb	7.19	803
Re	1.698	198
Ru	0.49	66
Sn	3.72	305
Ta	4.48	830
Tc	7.77	1410
Th	1.368	162
Ti	0.39	100
Tl	2.39	171
U χ	0.68	--
γ	1.80	--
V	5.30	1020
W	0.012	1
Zn	0.875	53
Zr	0.65	47

Table 2.1: The values of *Tc* and *Hc* for the superconducting elements

There are a lot of superconductors. Half of the metallic elements have got the properties of superconductivity. Moreover, a great number of alloys are superconductors. Although some alloys are composed of two metals which are not themselves superconductors such as Bi- Pd, they can be a superconductor.

	Nb	Pb	Ta	Sn	Zr
T_c(K)	9.3	7.2	4.5	3.7	0.8

	Ta-Nb	Pb-Bi	Nb_3-Zr	Nb_3Sn	Nb_3Ge
T_c(K)	6.3	8	11	18	23

Table 2.2: Superconducting Transition Temperatures of Some Alloys and Metalic Compounds Compared With Their Constituent Elements.

There may be some differences at the transition temperature of superconductors due to the fact that if the sample is pure or not. If the sample is pure and physically perfect on cooling, there can be extremely sharp transition to the superconducting state. For example in a good gallium specimen, the transition has been observed to occur within a temperature range 10^{-5} degrees. On the other hand, if the specimen has impurity or has a disturbed crystal structure the transition may be greatly enlarged **[6].**

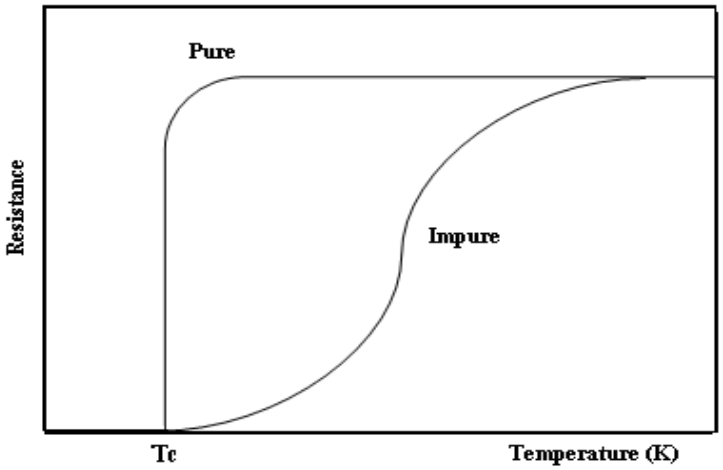

Figure 2.1: The transition temperature for pure and impure superconductor metals

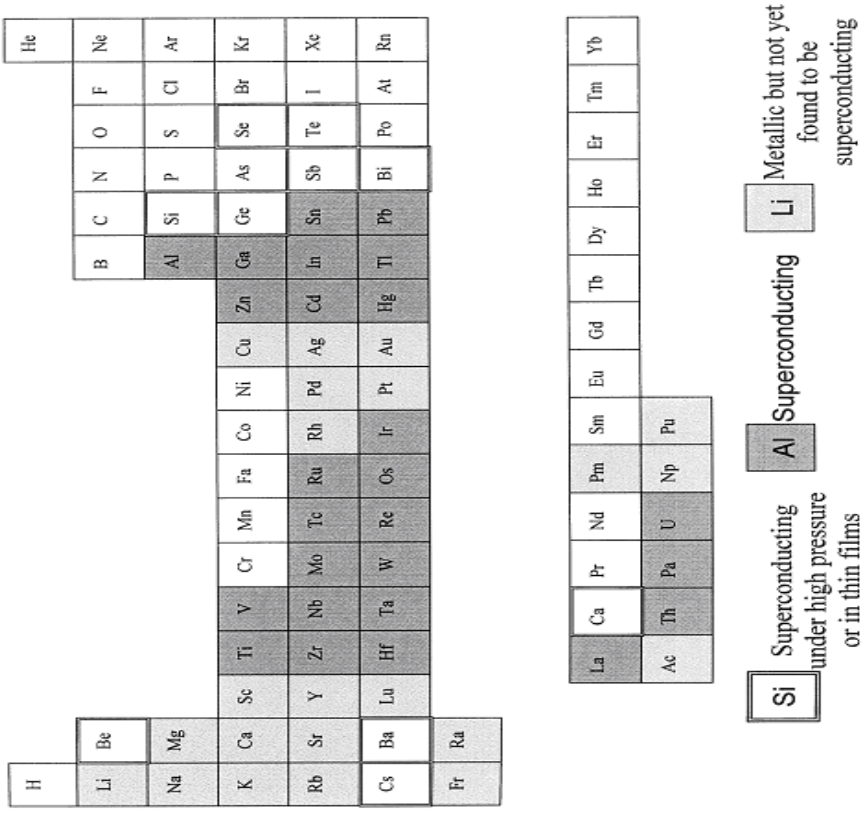

Table 2.3: Superconducting elements

2.3 NO RESISTIVITY

Zero resistivity or infinite conductivity is obtained in a superconductor at all temperatures below a critical temperature, T_c as shown in Figure 2.2. However, if we pass temperatures below a critical current density J_c, superconductivity occurs.

$$\rho = 0 \text{ for all } T < T_c$$

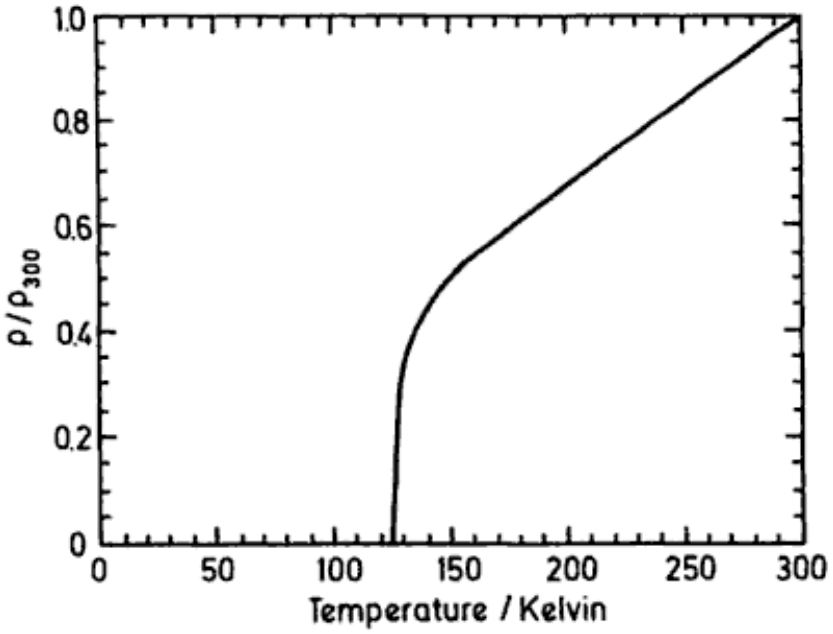

Figure 2.2: Temperature dependence of electrical resistivity of the oxide superconductor $Tl_2Ba_2Ca_2Cu_3O_{10}$ **[2].**

The zero resistivity of a superconductor can be measured to direct current. A major way to show zero resisitivity is to induce a current around a closed ring of a superconducting metal. Experiments have been displayed in which a ‘persistent

current' has run for over two and a half years without any measurable decay. In other words, the resistivity of a superconductor is smaller than 10^{-23} Ωm. This means that it is some 18 orders of magnitude smaller than the resistivity of copper at room temperature **[2].**

2.4 NO MAGNETIC INDUCTION

The magnetic inductance becomes zero inside the superconductor when the temperature of the superconductor metal is below T_c in a weak external magnetic field. This implies that the magnetic flux is expelled form the interior of the superconductor (Figure 2.3) **[2].**

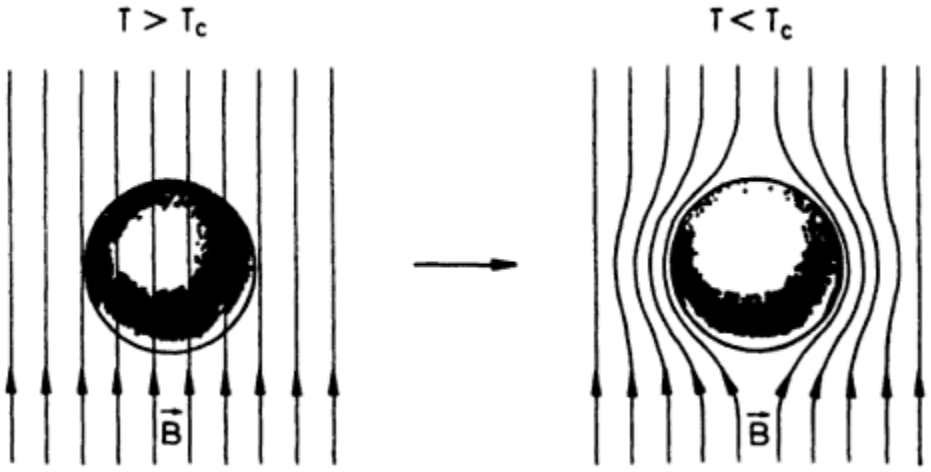

Figure 2.3: Expulsion of a weak, external magnetic field from the interior of the superconducting material **[2].**

2.5 MEISSNER EFFECT

As mentioned above, the Meissner effect is the expulsion of a magnetic field from within a superconductor (Figure 2.3). This expulsion is different from only not allowing in an external field. Any metal which has infinite conductivity would do the latter. If a magnetic field is already present, and a substance is cooled through T_c in order to obtain a superconductor. And, the magnetic field is expelled. The important of the difference is that the Meissner effect is valid only for superconductors **[4].**

The above phenomenon can be demonstrated by a few basic formula of electrodynamics.

$$\text{Ohm's law, } V=RI,$$

$$E=\rho J \ ,$$

where E represents the electric field, ρ the resistivity and J the electrical current density in the specimen. Zero resistivity shows zero electric field. Hence, if the Maxwell equation is taken;

$$\text{curl } E=-\ \partial B/\partial t$$

we obtain

$$\partial B/\partial t=0$$

It is seen that the magnetic induction in the interior of the specimen has to be constant as a function of time. There would be a main difference in the final state of the specimen if it was cooled under an applied external field or if the field was applied after the sample has been cooled below T_c. The field would have remained with in the sample in the first case whereas, in the second it would have been zero. The superconducting metal always expels the field from its interior independent of the precise sequence of cooling or applying the field for the specimen to be in the same thermodynamic state, and has $B=0$ in its interior. For this reason, the superconducting state is a true thermodynamic state because of the expulsion of the magnetic field **[2].**

2.6 COMPARISON BETWEEN A SUPERCONDUCTOR AND A VERY GOOD (OR IDEAL) CONDUCTOR

A perfect conductor does not display Meissner effect. In other words, no flux expulsion on cooling.

There is a striking difference between a perfect conductor and a superconductor. The demonstrated magnetic behaviour of an ideal conductor relates to on whether the sample is first cooled to below T_c before applying the field (1) or the field is applied and then cooled (2). But, the final states are the same, regardless of whether B_{ext} is switched on before, or after cooling for a superconductor **[7].**

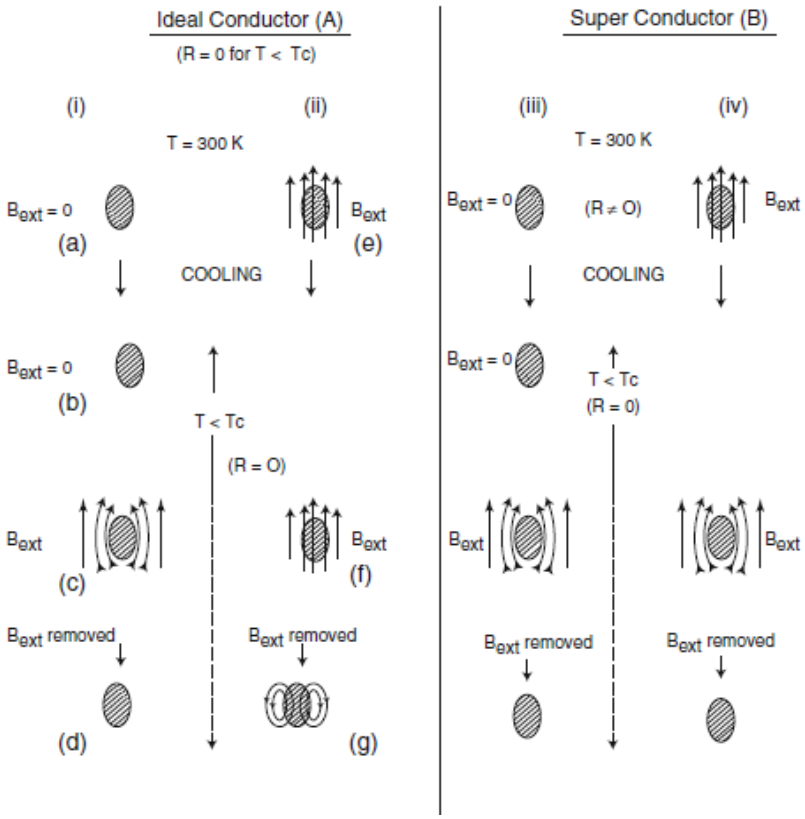

Figure 2.4: Comparison of magnetic behaviours of an ideal conductor and a superconductor. Both have $R=0$ for $T<T_c$ **[7].**

In Figure 6 part (i), an ideal conductor is cooled to below the critical temperature without magnetic field. When a magnetic field is applied, currents are induced in the surface, and when the field is removed, the field within the material remains at zero. On the other hand, part (ii) indicates that if an ideal conductor is cooled to below its critical temperature in a uniform magnetic field, a situation where the uniform field is maintained within the material. On condition that the applied field is then removed, the field within the conductor does not disapper, and the continuity of magnetic field lines show that there is a field in the region around the ideal conductor. There is a significant point is that the magnetization

state of the ideal conductor depends not only on temperature and magnetic field, but also on the previous history of the material.

In contrast, when a superconductor material is cooled to below its superconductor critical temperature in zero field or in a finite field, the magnetic field within a superconducting material is always zero as shown in part (iii) and part (iv) of the same figure. The magnetic field is always expelled from a superconductor. This is carried out spontaneously by producing currents on the surface of the superconductor. A magnetic field is created due to the direction of that currents. The external magnetic field and the created magnetic field by the superconductor exactly cancels each other. It is called as the Meissner effect, that distinguishes a superconductor from an ideal conductor at zero resistance. It is obvious that the state of magnetization of an ideal conductor depends on the sequence by which external conditions were carried out **[6].** Hence, zero resistance and zero magnetic field are the major properties of superconductivity.

2.7 TYPE I SUPERCONDUCTORS

Superconducting samples that completely expel magnetic flux until they reach normal state are called type-I superconductors. According to the older literature, they were referred to as ‘soft’ or ‘pure’ superconductors., all superconducting elements and most of superconducting alloys in the ‘dilute limit’, are type-I superconductors exceptionally V and Nb. The strength of the applied magnetic field needed to completely damage the state of perfect diamagnetism within the superconducting material is called the thermodynamic critical magnetic field written as B_c. As shown in below (Figure 2.5), the chancing of the critical

magnetic field B_c with the temperature is almost parabolic for type I superconductor.

$$B_c = B_0 \left\{ 1 - \left(\frac{T}{T_c} \right)^2 \right\}$$

The value of B_0 is the extrapolated value of B_c at $T=0$ **[2].**

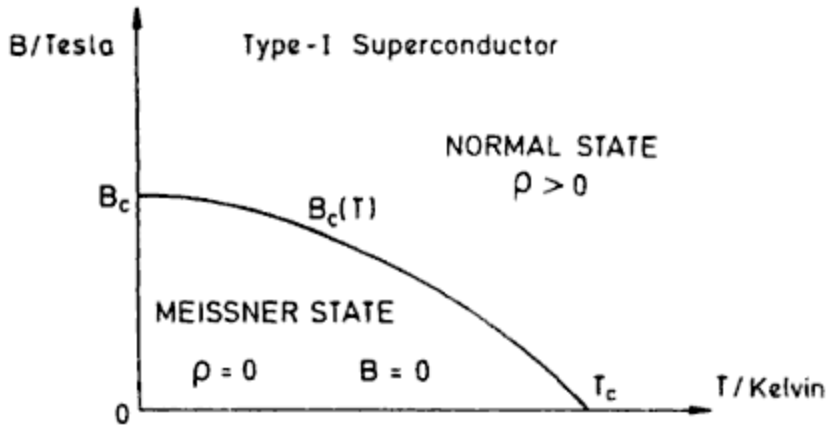

Figure 2.5: Schematic diagram of $B_c(T)$ for type-I superconductor **[2].**

2.8 TYPE II SUPERCONDUCTORS

Type-II superconductors has two critical magnetic fields which are called as lower critical magnetic field B_{c1} and upper critical magnetic field B_{c2}. The magnetic flux is fully expelled up to the lower critical magnetic field B_{c1}. Therefore, if the applied magnetic fields is smaller than B_{c1}, the type-II superconductor behaves just like a type-I superconductor. However, if the applied magnetic fields is larger than B_{c1}, the magnetic flux partially penetrates into the

material up to the upper critical field, B_{c2}. And, if the applied magnetic fields is above B_{c2} , the material lose the property of superconductivity, and returns to the normal state (see Figure 2.6b).

The superconductor is said to be in the mixed state if the applied magnetic field is between B_{c1} and B_{c2}. The Meissner effect is observed partially. In the mixed state, magnetic flux partially penetrates the superconducting sample in the form of tiny microscopic filaments called vortices (Figure 2.6) **[2].**

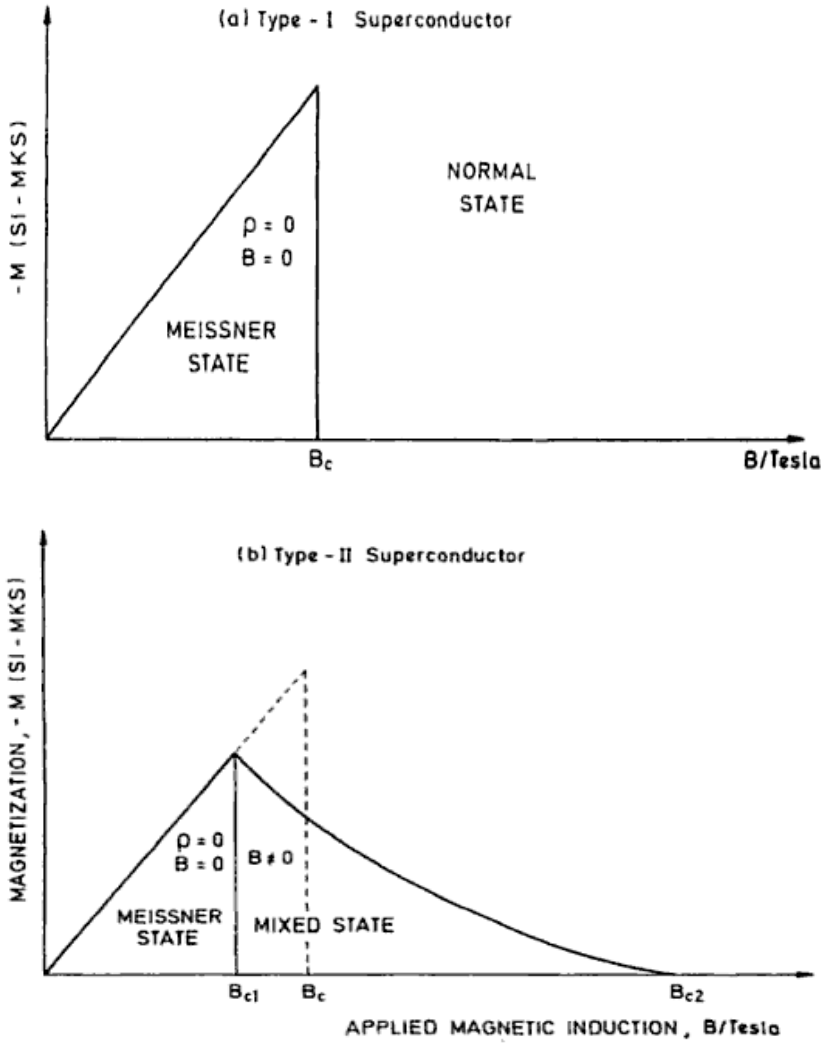

Figure 2.6: Variation of magnetization as a function of the magnetic field for (a) type-I superconductor and (b) type-II superconductor **[2].**

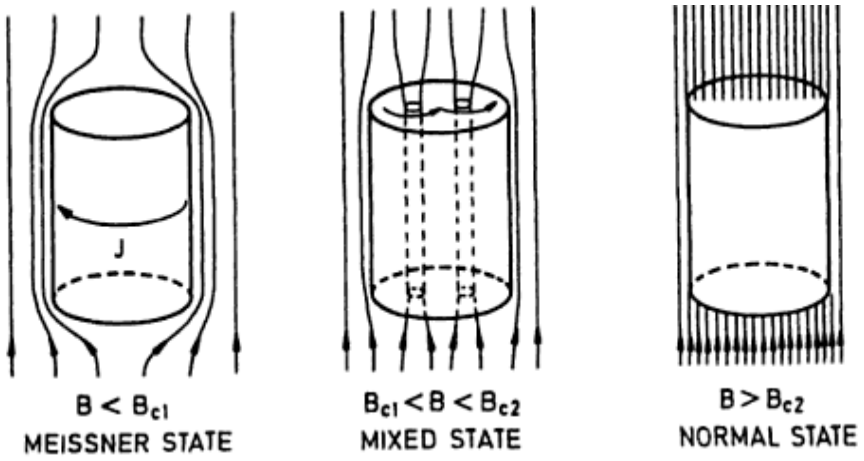

Figure 2.7: Flux penetration in the mixed state (after Decroux and Fischer 1989) **[2].**

2.9 PENETRATION DEPTH

A measure of how deep light or any electromagnetic radiation can penetrate into a material is called penetration depth. In other words, the depth at which the intensity of the radiation inside the material falls to 1/e (about 37%) of the original value at the surface is defined as penetration depth.

Magnetic field is equal to zero (B=0) in the interior of a superconductor due to the Meissner effect. However, this effect cannot be seen at the surface of the superconductor. In fact, there should be currents on the surface which give rise to magnetization M in order to cancel B so that in the interior of the superconductor $M+H=0$. These surface currents do not dissipate energy when the resistivity is zero, and it is called superfluid currents or simply supercurrents. The thickness of the region of the material (measured from the surface) though which

flow the supercurrents are called the penetration depth of the magnetic field, λ. It is a characteristic property (lengths) which characterize the superconductor **[6].**

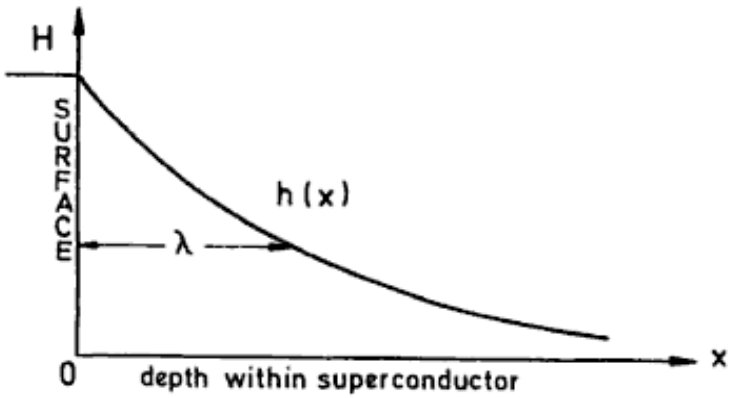

Figure 2.8: Schematic decay of magnetic field in the interior of a superconductor **[2].**

2.10 COHERENCE LENGTH

Coherence length ($\xi 0$) is defined as the maximum distance between electrons of a cooper-pair in real space up to which their motion is correlated (by taking advantage of the attractive interaction).

Both coherence length and penetration depth diverge likewise near $T = T_c$. Hence, a constant k is defined as

$$k = \lambda/\xi,$$

which will remain finite as $T \rightarrow T_c$.

It is called as Ginzburg–Landau parameter and can be considered as a characteristic of a material. The magnitude of k defines two kinds of

superconductors. For $k << 1$ (i.e. $\lambda << \xi$), type-I superconductors are obtained and superconductors having $k >> 1$ (i.e. $\lambda >> \xi$) are type II superconductors **[7].**

2.11 $Bi_2(Pb)Sr_2Ca_{n-1}Cu_nO_x$ (n=1, 2, 3) SUPERCONDUCTOR

Bismuth strontium calcium copper oxide (BSCCO) is a family of high temperature superconductors. Its chemical formula can be written as $Bi_2Sr_2Ca_{n-1}Cu_nO_x$, with n=1,2,3 **[11].**

There is a wide area in order to study on this family of superconductor. Because this family does not consist of poison elements or rare earth elements. Moreover, Bi-based superconductors are very useful for applications in technology and industry.

Superconductivity in *Bi-Sr-Cu-O* system was discovered by Michel et al. in 1997 **[8].** Then, bismuth $(Bi_2Sr_2Ca_2Cu_3O_{10+\square})$ and thallium $(Tl_2Ba_2Ca_2Cu_3O_{10+\square})$ based superconductors with even higher T_c were discovered. In 1988, Ca was added to this system and *Bi-Sr-Ca-Cu-O* was produced with a high *Tc* of about 105 K by Meada et al **[9].** Later, some researches were carried out so as to obtain zero resistance at high temperatures. In 1908, Pb was added to this system and obtained superconductivity onset temperature at 110 K and achieved a stable superconductor by Takano et al. **[10].**

There are three phases of $Bi_2(Pb)Sr_2Ca_{n-1}Cu_nO_x$ superconductor as $Bi_2Sr_2Cu_1O_x$ (2201), $Bi_2Sr_2Ca_1Cu_2O_x$ (2212), *and* $Bi_2Sr_2Ca_2Cu_3O_x$ (2223). Each of them has diffrent crystal structures. Their transition temperatures (T_c) are seen at 5

K, 85 K and 110 K for $Bi_2Sr_2Cu_1O_x$ (2201), $Bi_2Sr_2Ca_1Cu_2O_x$ (2212), and $Bi_2Sr_2Ca_2Cu_3O_x$ (2223), respectively **[21].**

2.12 CRYSTAL STRUCTURE OF THE $Bi_2Sr_2Ca_{n-1}Cu_nO_x$ (*n*=1, 2, 3) SYSTEM

The form of $Bi_2Sr_2Ca_{n-1}Cu_nO_x$ is obtained by crystallizing Bi-based high temperature superconductors **[11].** Here, n is the number of cupper-oxide layers in the range of 1,2,3. Moreover, if n increases, T_c also increases **[21].**

2.12.1 Crystal Structure of the $Bi_2Sr_2CuO_6$ (2201) System

$Bi_2Sr_2CuO_6$ (2201) compound which was first discovered by Michel et al. in 1987 has the lowest T_c (0-20 K) of the Bi-based superconductors. It has a tetragonal symmetry with lattice parameters $a = b = 5.39$ °A, $c = 24.6$ °A **[11].** The unit cell of $Bi_2Sr_2CuO_6$ is shown in Figure 2.9 **[12].**

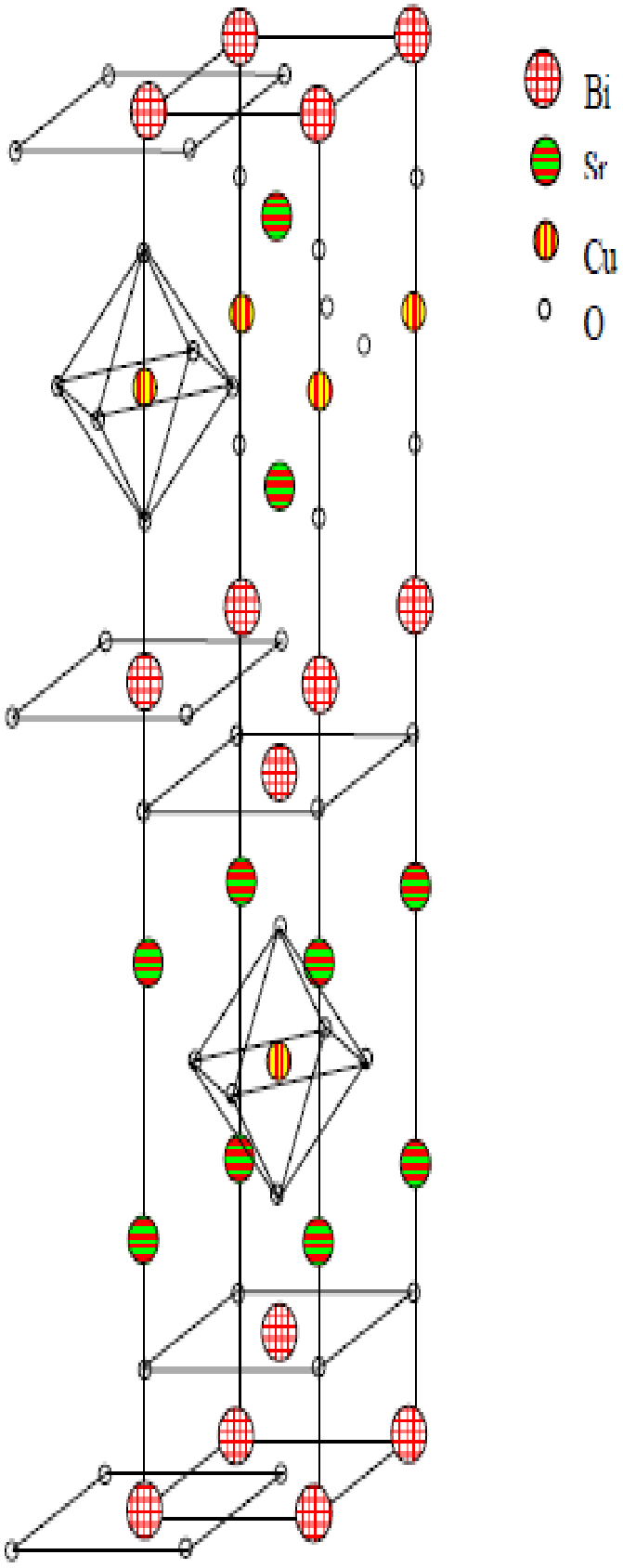

Figure 2.9: Crystal structure of $Bi_2Sr_2CuO_6$ compounds **[12].**

2.12.2 Crystal Structure of the $Bi_2Sr_2CaCu_2O_8$ (2212) System

$Bi_2Sr_2CaCu_2O_8$ compound was generated by the way of adding of Ca to $Bi_2Sr_2CaCu_2O_6$ system by Maeda et al. It has pseudo-tetragonal crystal structure with lattice parameters $a = b = 5.4$ °A, and $c = 30.6$ °A. This compound also known as 2212 phase for $n = 2$ in $Bi_2Sr_2Ca_{n-1}Cu_nO_x$ form has a critical transition temperature 75-85 K **[11].** Figure 2.10 shows the crystal structure of $Bi_2Sr_2CaCu_2O_8$ compound **[12].**

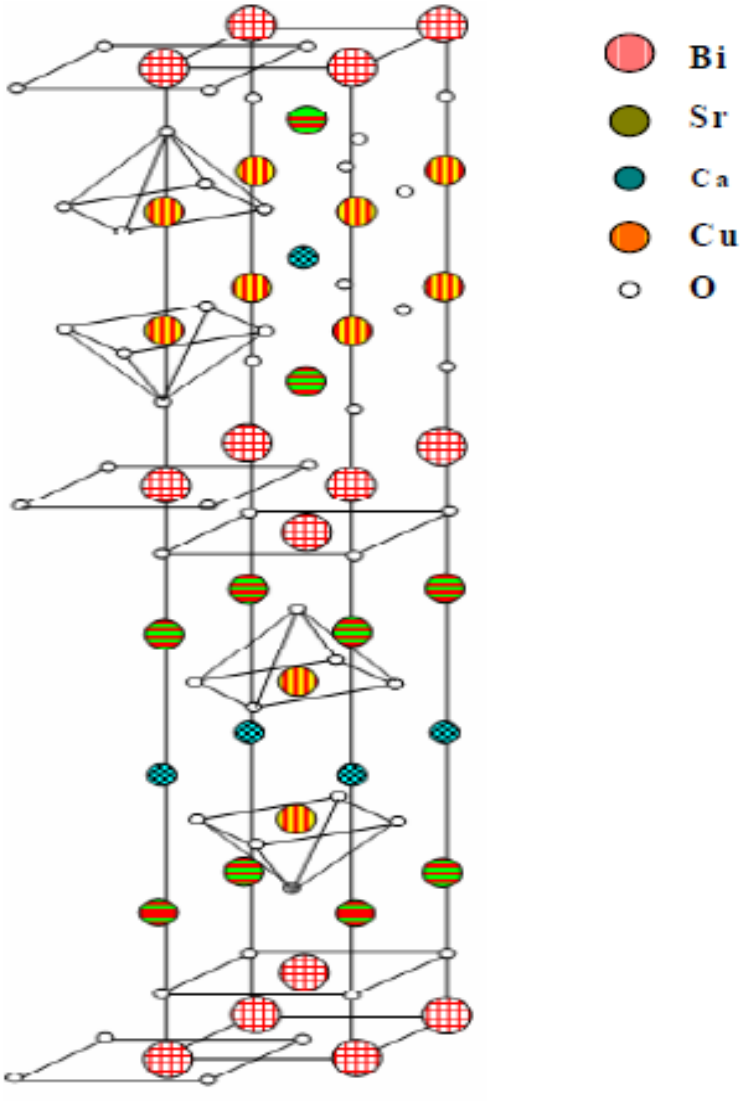

Figure 2.10: Crystal structure of $Bi_2Sr_2CaCu_2O_8$ compounds **[12].**

2.12.3 Crystal Structure of the $Bi_2Sr_2Ca_2Cu_3O_{10}$ (2223) System

The form of $Bi_2Sr_2Ca_2Cu_3O_{10}$ (2223) compound is pseudo-tetragonal structure with T_c at 110 K. It includes two Bi-O layers, two Sr-O layers, two Ca and three Cu-O layers **[13].** That system has got the highest T_c and, it consists of same kinds of atoms of $Bi_2Sr_2CaCu_2O_8$ (2212) system. The c value is increased to 37.1 °A by adding one Ca and one Cu-O_2 layer to the structure of BSCCO-2212 phase. Figure 2.11 represents the crystal structure of Bi-2223 phase **[12].**

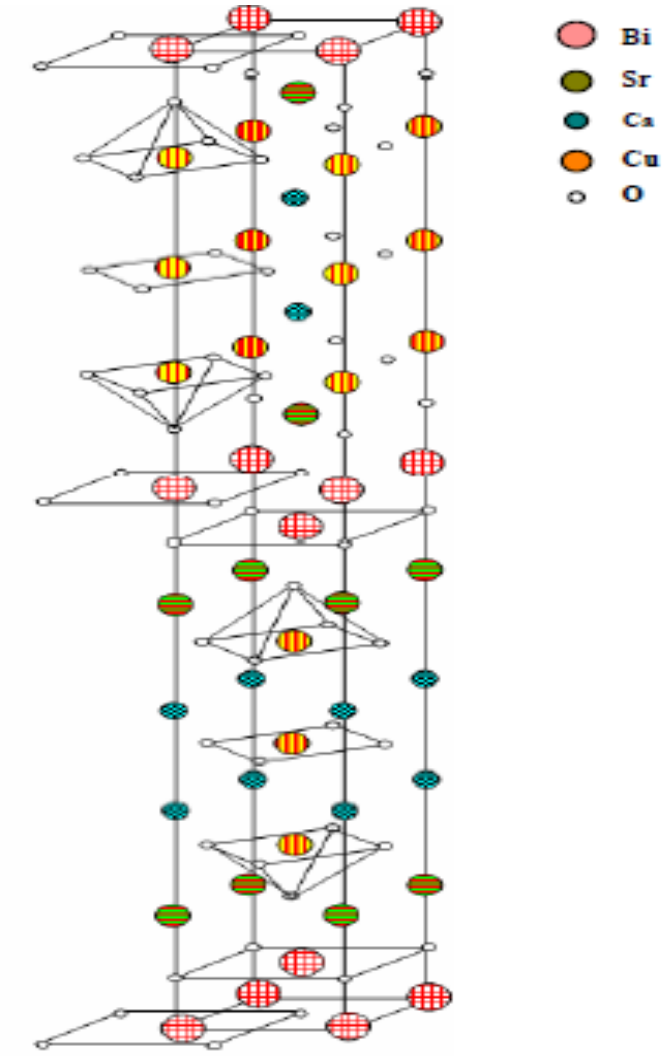

Figure 2.11: Crystal structure of $Bi_2Sr_2Ca_2Cu_3O_{10}$ compounds **[12].**

CHAPTER 3

EXPERIMENTAL METHOD

3.1 PREPARATION OF THE BSCCO THIN FILM SAMPLE

The films are prepared by DC sputtering method. Firstly we have prepared the target by using the following powders $Bi2O_3$ (purity 99.99%), *PbO* (purity 99.9+%), $SrCO_3$ (purity 99.9+%), $CaCO_3$ (purity 99+%) and *CuO* (purity 99+%). They were mixed in the stoichiometric ratios of Bi:Pb:Sr:Ca:Cu:O=2:1:2:1.6:2.2:8 and the compound were determined as below:

Element	Atomic Weight (au)
Bi	208.98
Pb	207.19
Sr	87.62
Ca	40.08
Cu	63.54
C	12.01
O	15.99

COMPOUNDS	PURITY (%)	ATOMIC WEIGHT
Bi_2O_3	99.99%	465.96
PbO	99.9+%	223.19
$SrCO_3$	99.9+%	147.63
$CaCO_3$	99+%	56.08
CuO	99+%	79.54

Table 3.1: Atomic weights of the compounds.

Hence, the chemical equation can be written as below;

$$Bi_2O_3 + PbO + 2\ SrCO_3 + 1.6\ CaCO_3 + 2.2\ CuO + \rightarrow Bi_2Pb_1Sr_2Ca_{1.6}Cu_{2.2}O_x + \text{gases}$$

From this equation, the quantities of reactants are calculated to produce approximately 50 grams of mixture powder. They are shown in Table 3.2.

COMPOUNDS	MASS (gr)
Bi_2O_3	18.651 (gr)
PbO	8.793 (gr)
$SrCO_3$	11.632 (gr)
$CaCO_3$	3.535 (gr)
CuO	6.894 (gr)

Table 3.2: The weight of the compounds for produce 50 grams

At first, all of these compounds (Table 3.2) were weighted by using a sensitive balance (Figure 3.1) and were thoroughly mixed for 24 hours with a rotation speed of 2000 rpm in 10 min under air in a grinding machine to obtain a target. After obtaining homogenous mixture, it was subjected to calcining process at 800°C for 12 hours in muffle furnace (Figure 3.2) with 5^0C per minute heating rate, and cooled down to room temperature with 5^0C per minute cooling rate. Then, it was pelletized into cylindrical bars at 260 MPa by using press machine. (Figure 3.3) The cylindrical target with a thickness of 4 mm was obtained to be about 5 cm in diameter. The target was annealed at 830°C for 12 hours with 5^0C per minute heating and cooling rate in air in same furnace. The target was sticked to a copper backing plate using silver paste. Then, it was placed on the dc gun in the sputtering system.

Figure 3.1: XR 205SM-DR Precisa balance

Figure 3.2: PROTHERM (Model PTF 12/75/200) programmable tube furnace

Figure 3.3: TSEK TÜMAS press machine

3.1.1 DC Sputter System

Sputtering is a process whereby atoms are ejected from a solid target material due to bombardment of the target by energetic particles **[14].** It is usually used for thin film deposition, etching and analytical techniques.

Free electrons are accelerated away from the negatively charged electrode (cathode). These accelerated electrons collide the neutral gas atoms in their path. And, the gas atoms have more positively charged protons than negatively charged electrons. Hence, they are not any more a neutral gas atom but a positively charged "ion" (e.g. Ar +). This positively charged ions are accelerated into the

negatively charged electrode (cathode=target). Meanwhile these ions strike the target, the electrons of which are started to ejected. When these electrons return to a ground state because of the conservation of energy law, the resultant neutral gas atoms gain energy and must release that same energy in the form of a photon. The release of these photons is the reason the plasma appears to be glowing.

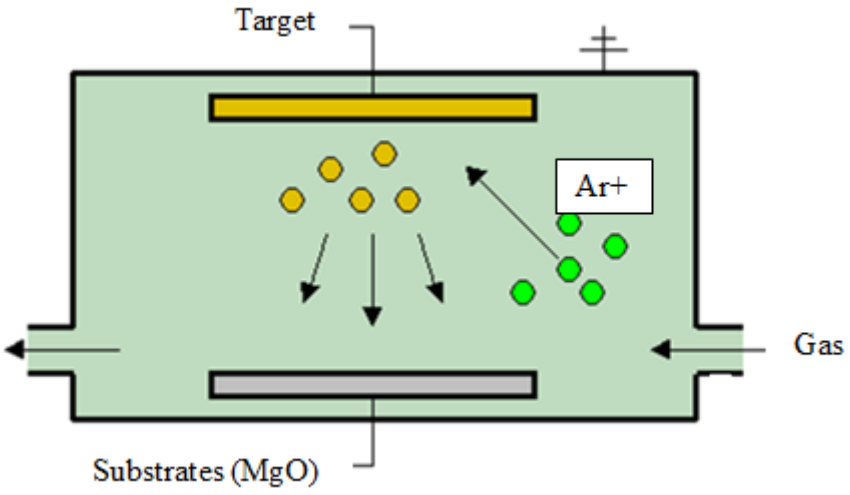

Figure 3.4: Schematic diagram of a DC sputter.

BSCCO thin films were deposited on the one-side polished substrates, MgO (100), by the NSC-3000 Sputter Coater at 100 W DC power. Before film fabrication process, the substrates were ultrasonically cleaned by acetone and deionized water and then dried by way of nitrogenous gas. The cleaned substrates were placed on a hot plate (70 °C) in Sputter Coater and the temperature of the substrates were maintained at 70 °C during the film sputtering process. The air in chamber of sputter coater was evacuated up to 4.75×10^{-6} torr by means of the rotary (Figure 3.6). However, the pressure was recorded to be about 3.78×10^{-3} torr with the beginning of the fabrication process. Then, 40 sccm Ar gas flow was

used for plasma state and 100 W DC power was adjusted to apply to the samples for this process. The distance between target and substrates was adjusted to be about 5 cm. The film production process was 6 hours. At the end of the process, the films were taken out from the sputtering machine. They appeared as shining and dark (Figure 3.8).

Figure 3.5: Air compressor 230 VAC.

Figure 3.6: Edwards rotary.

Figure 3.7: NSC-3000 sputter coater nano-master, Inc.

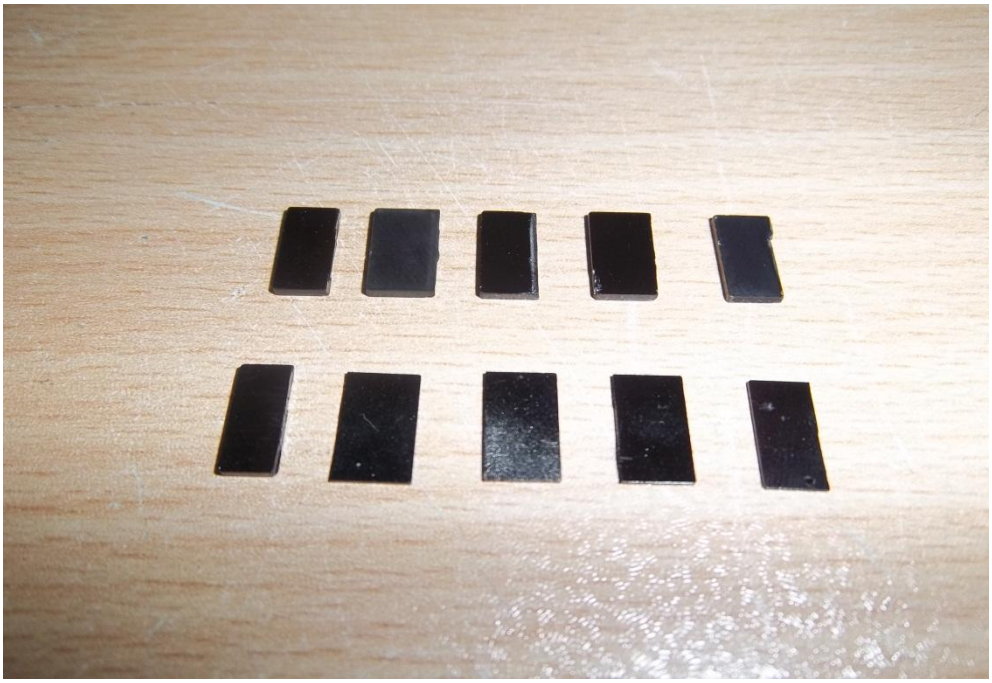

Figure 3.8: BSCCO thin films.

We produced ten superconductor thin films (Figure 3.8). Five of the fabricated amorphous films were placed in furnace for annealing in air one by one. The annealing process included two steps. In the first step, they were sintered at 800 ^{0}C for 1 hour in furnace with 5 ^{0}C per minute heating rate. Then, they were subjected to second annealing process at 840 ^{0}C for different hours (1,2,4,6 and 8) with 1 ^{0}C per minute heating rate and then, cooled down to room temperature with 5 ^{0}C per minute cooling rate. On the other hand, the other films were annealed in the second step at 850 ^{0}C with the same annealing procedure and same annealing times. The sintering process is shown in below as a graph (Figure 3.9).

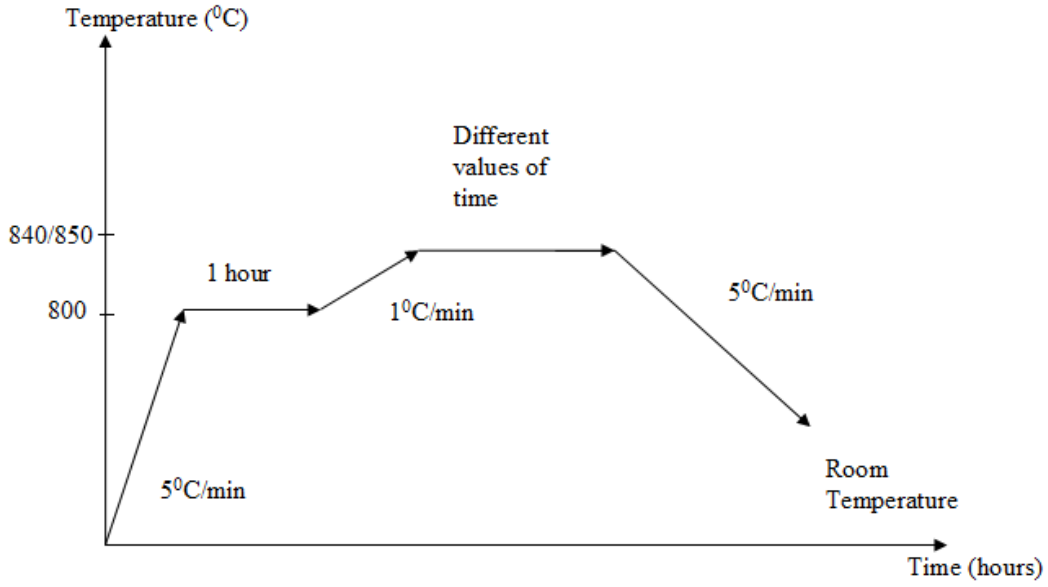

Figure 3.9: Sintering process of the samples.

3.1.2 X-Ray Diffractometer

A diffractometer is a measuring instrument for analyzing the structure of a material from the scattering pattern produced when a beam of radiation or particles (as X rays or neutrons) interacts with it.

Figure 3.10: Rigaku X-Ray diffractometer.

X-ray diffraction (XRD) data were taken using a Rigaku D/Max-IIIC diffractometer with CuK_{α} radiation in the range $2\Theta = 3°$- 60° with a scan speed of 3 °/min and a step increment of 0.02° at room temperature. The XRD measurements provide data about lattice parameters, average crystallize size and phase purity for the samples produced in this work.

3.1.3 Scanning Electron Microscope

The scanning electron microscope (SEM) is a kind of electron microscope. It images the sample surface by scanning with a high-energy beam of electrons in a raster scan pattern. The electrons interact with the atoms that make up the sample producing signals that contain information about the samples' surface topography, composition and other properties such as electrical conductivity.

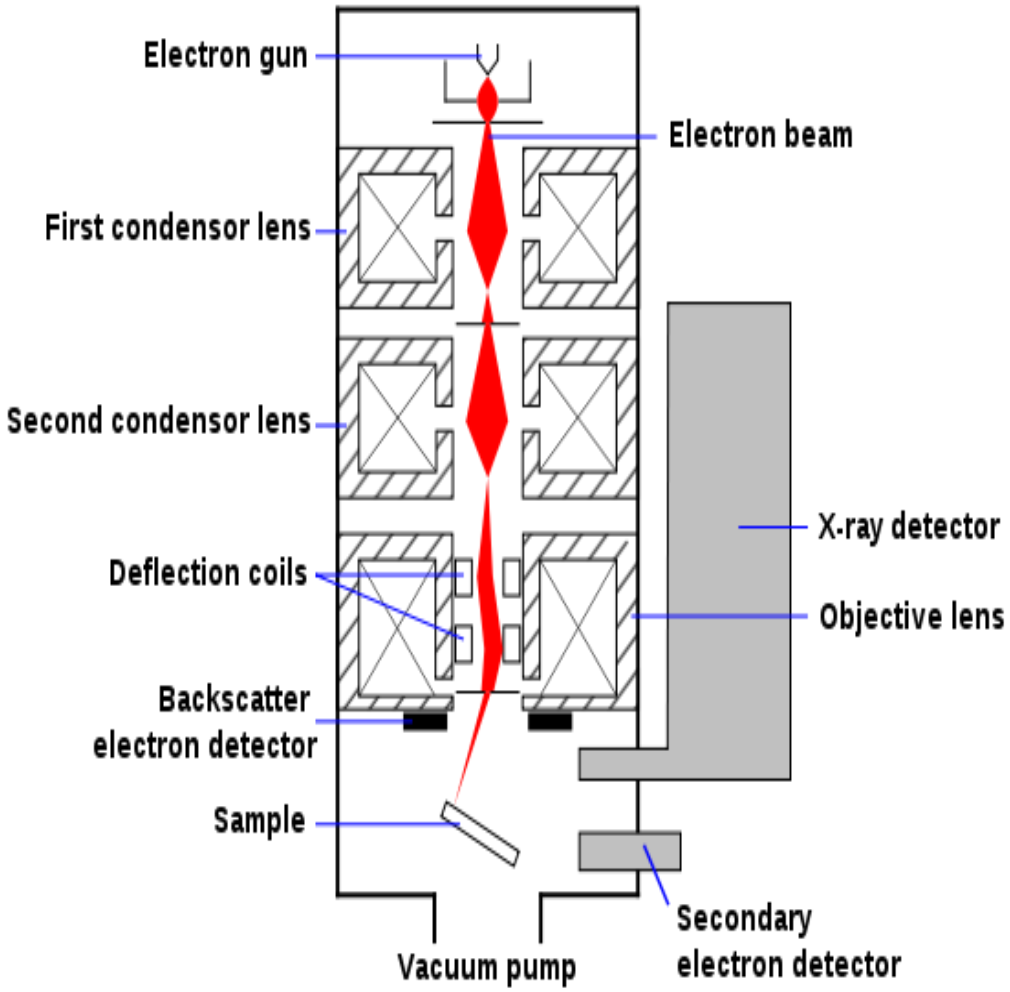

Figure 3.11: Schematic diagram of a SEM.

In the next step, the surface morphology of the superconducting films was examined by scanning electron microscopy (SEM).

Figure 3.12: JEOL JSM-6390LV scanning electron microscope.

3.1.4 Energy Dispersive Spectrum Analysis

Energy-dispersive spectroscopy (EDS) is an analytical method. It is used for the elemental analysis or chemical characterization of a substance. It investigates not only a sample through interactions between electromagnetic radiation and matter but also X-rays emitted by the matter in response to being hit with charged particles. Atomic structure of the elements can be identified uniquely from one another due to unique atomic structure.

A high-energy beam of charged particles are focused on a specimen. At rest, an atom within the specimen has ground state (or unexcited) electrons in discrete energy levels or electron shells bound to the nucleus. The incident beam can excite an electron in an inner shell of an atom, ejecting it from the shell and creating a hole. An electron from an outer, higher-energy shell then, it fills the hole. The difference in energy between the higher-energy shell and the lower energy shell can be released in the form of a photon. The number and energy of the photon emitted from a sample can be measured by an energy-dispersive spectrometer. While the energy of the photon is characteristic of the difference in energy between the two shells, and of the atomic structure of the element from which they were emitted, this shows the elemental composition of the sample to be measured.

3.1.5 Cryocooler

In final step, resistivity versus temperature measurements of the films were carried out between 30–120 K by means of Helium gas contact crycooler from CRYO Industries (Figure 3.13, 3.14, 3.15 and 3.16). Both voltage and current contacts were made with silver paint for resistivity measurements. Cernox temperature sensor was used to measure the temperature rise on the sample.

Moreover, magnetoresistivity measurements were carried out for only the film annealed at 840^0C for 2 hours. We measured temperature (30-120 K) and DC magnetic field (0.5, 1, 3 and 5 T) dependent of resistivity of the films with 1 mA DC current in a cryostat. The magnetic field was applied parallel and

perpendicular to the surface of the film. The transition temperature T_c was found as the temperature at zero resistivity.

Figure 3.13: Cryostat system.

Figure 3.14: Helium compressor.

Figure 3.15: Turbo molecular pump.

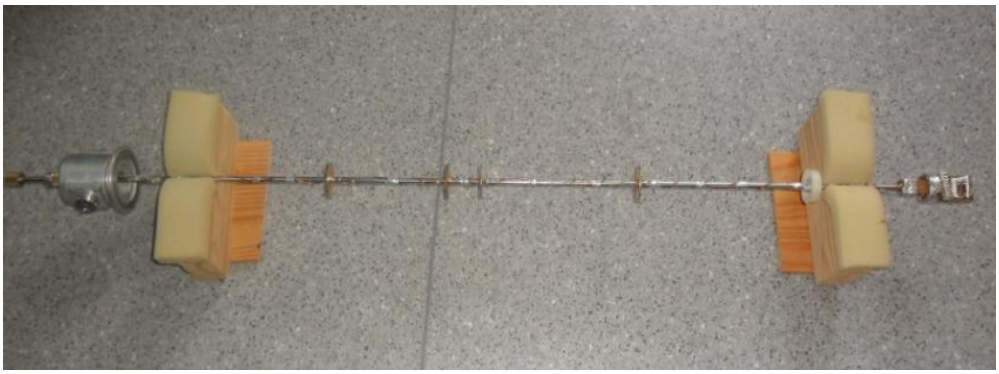

Figure 3.16: Measurement stick.

CHAPTER 4

RESULTS AND DISCUSSIONS

4.1 INTRODUCTION

In this chapter, resistivity mesurements, x-ray diffraction analysis, SEM (Scanning Electron Microscopy) photographs and EDS (Energy Dispersive Spectroscopy) analysis of Bi(Pb)SrCaCuO thin film samples were investigated, and the results of all measurements were discussed.

4.2 RESISTIVITY MEASUREMENTS

Resistivity versus temperature measurements of thin films were analyzed in this section. The electrical resistivity were measured by using the standard four-probe dc technique in the temperature range from 30 to 120 K with DC current of 1 mA. The values of T_c^{offset} were taken into account for comparison.

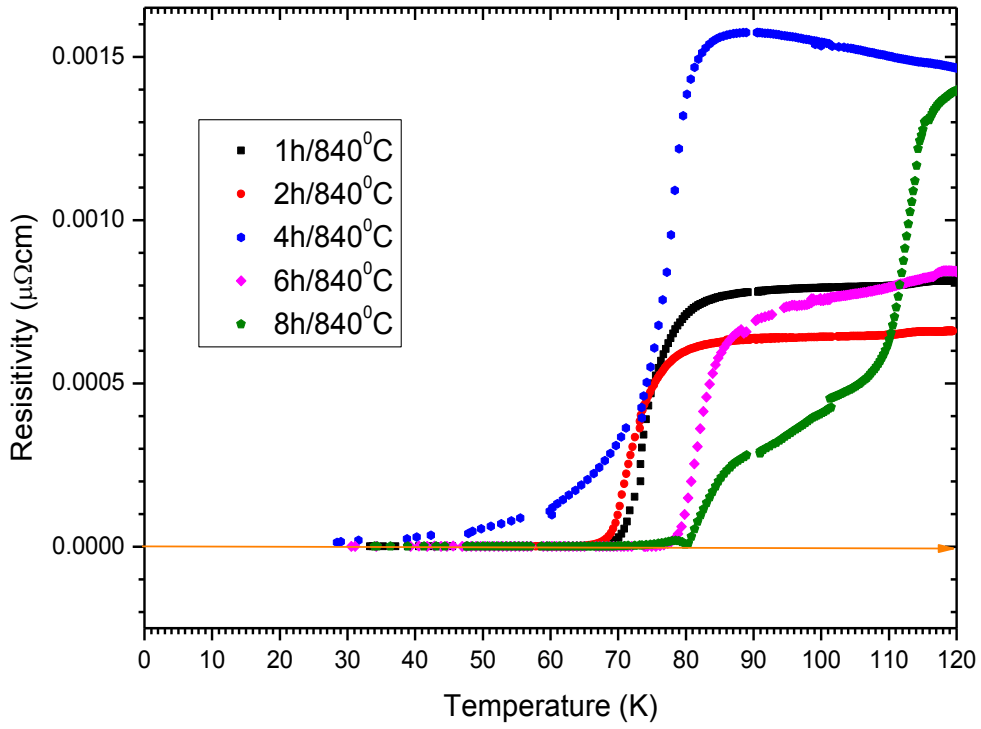

Figure 4.1: Resistivity versus temperature graph of Bi(Pb)SrCaCuO thin films annealed at 840^0C for 1,2,4,6 and 8 hours.

The critical temperatures of the films annealed at 840^0C with different deposition time are shown in Figure 4.1. As seen from the figure, the 8 hours annealed film was found to obtain the highest critical temperature with 81 K whereas the lowest critical temperature (69 K) was observed for the 2 hours annealed film. Based on these results, at 840^0C the 8 hours annealing process is suitable to the film obtaining higher critical temperature.

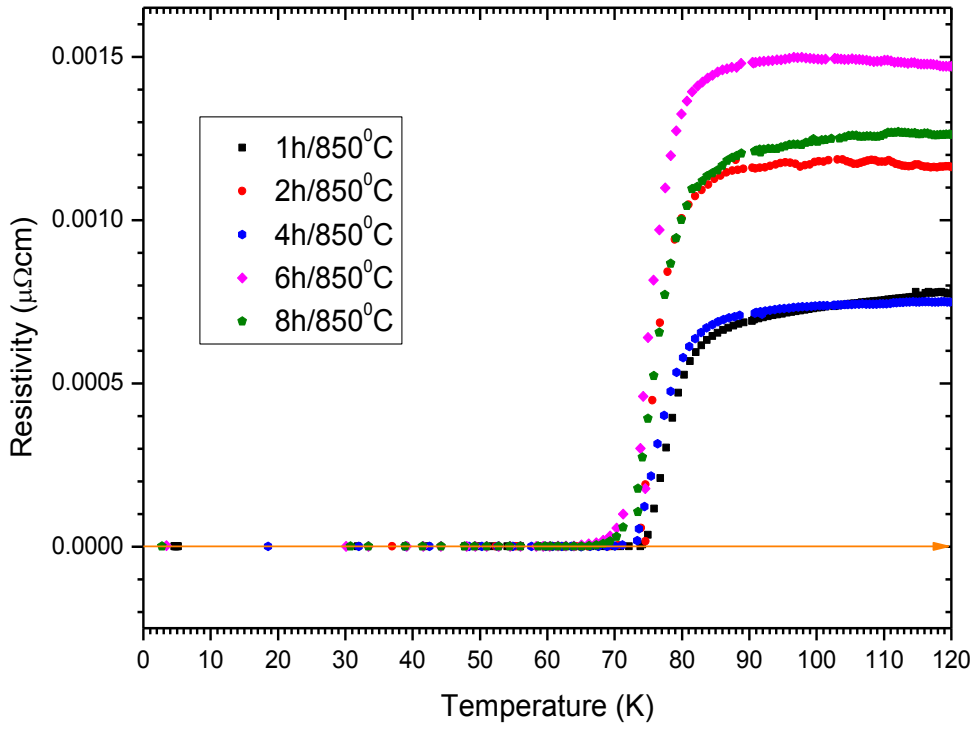

Figure 4.2: Resistivity versus temperature graph of Bi(Pb)SrCaCuO thin films annealed at 850^0C for 1,2,4,6 and 8 hours.

The critical temperatures of the films annealed at 850^0C are observed to be close to each other as shown in Figure 4.7. The highest value of the critical temperature was found to be about 75 K for the 1 hour annealed film. On the other hand, 70 K (the 6 hours annealed film) was obtained to be the lowest critical temperature. Contrary to the results of annealing process at 840^0C, the less annealing time the higher critical temperature is obtained.

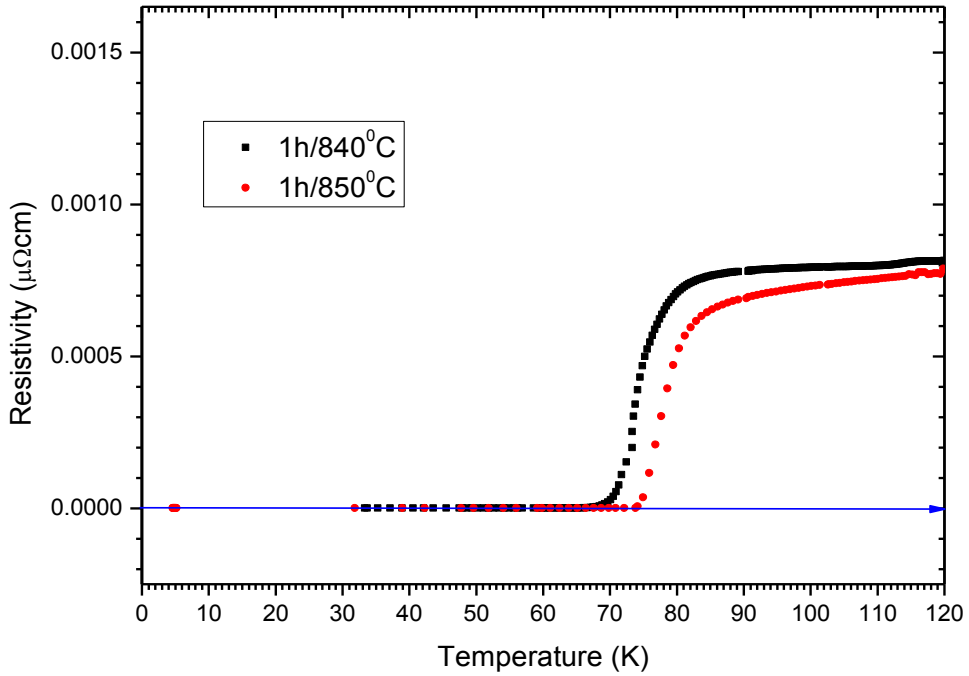

Figure 4.3: Resistivity versus temperature graph of Bi(Pb)SrCaCuO thin films annealed at 840^0C and 850^0C for 1 hour.

Figure 4.3 shows the resistivity versus temperature graph for the Bi(Pb)SrCaCuO thin film annealed at 840°C and 850^0C for 1 hour annealing time. As seen from the graph, off-set critical temperatures of the films annealed at 840°C and 850^0C were found to be about 71K and 75K, respectively. According to these results, the critical temperature was obtained to increase whereas the resistivity was noticed to decrease with the increase in the annealing temperature **[17].**

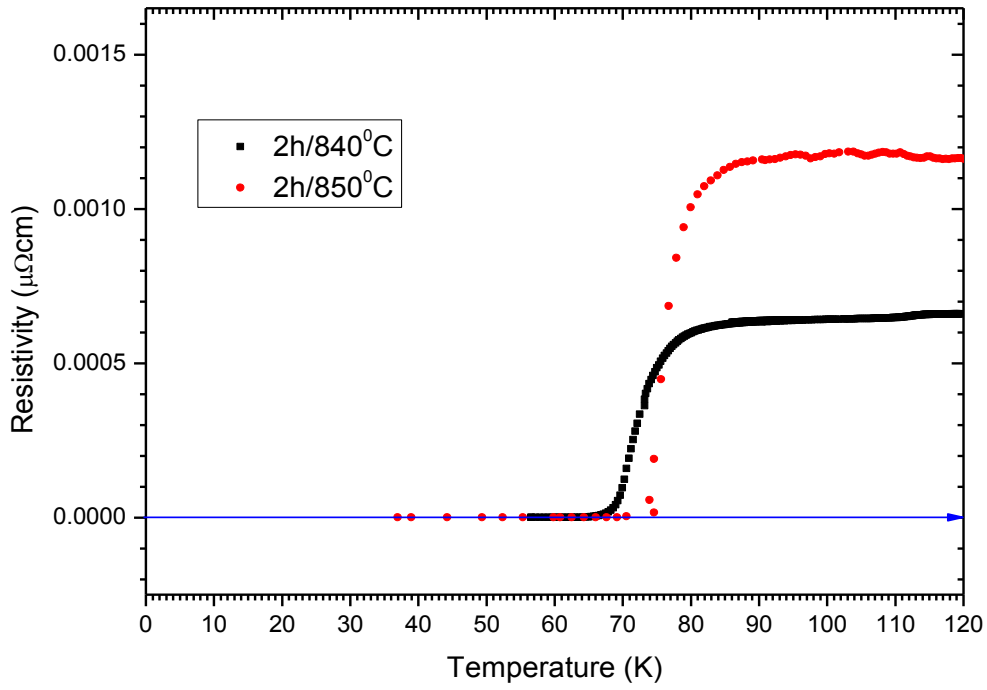

Figure 4.4: Resistivity versus temperature graph of Bi(Pb)SrCaCuO thin films annealed at 840^0C and 850^0C for 2 hours.

The following figure represents resistivity versus temperature graph of Bi(Pb)SrCaCuO thin films annealed at 840^0C and 850^0C for 2 hours. As shown above, critical temperatures of the films were obtained at 69K and 74 K for the films annealed at 840^0C and 850^0C, respectively. According to these values, it can be easily said that the more annealing temperature (for 2 hours annealing time), the more critical temperature we will obtain **[17].**

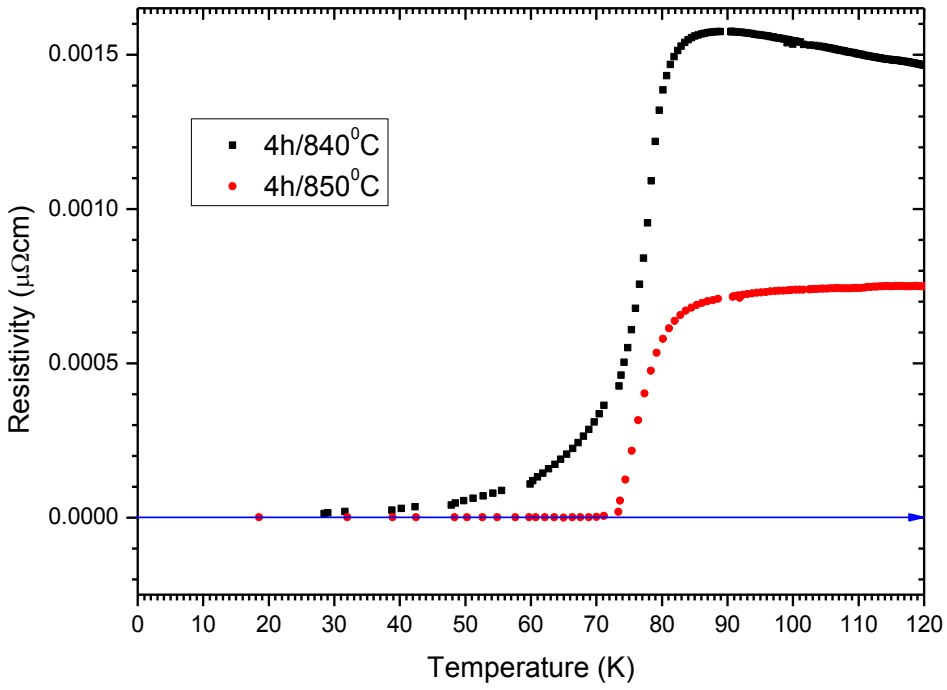

Figure 4.5: Resistivity versus temperature graph of Bi(Pb)SrCaCuO thin films annealed at 840^0C and 850^0C for 4 hours.

The Figure 4.5 is resistivity versus temperature graph of Bi(Pb)SrCaCuO thin films annealed at 840^0C and 850^0C for 4 hours. As seen from the figure, 71 K and 73 K were noted as critical temperatures of the films annealed at 840^0C and 850^0C, respectively. Based on these results, the critical temperature was obtained to increase with the increase of the annealing temperature. Furthermore, the film annealed at 840^0C exhibits the semiconductor behaviour as seen in the figure **[20].**

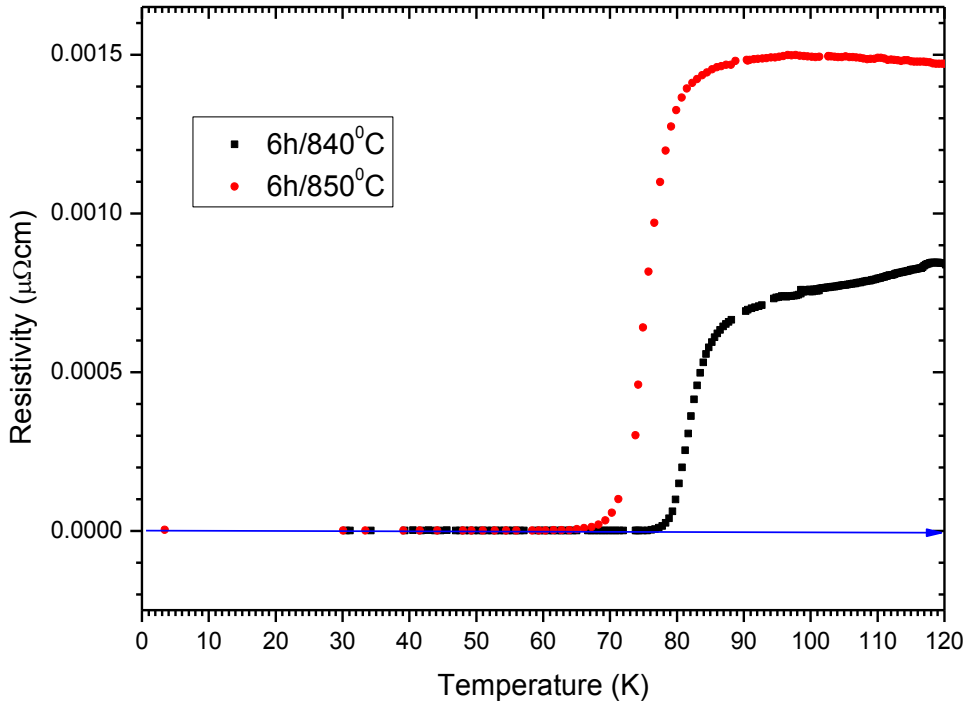

Figure 4.6: Resistivity versus temperature graph of Bi(Pb)SrCaCuO thin films annealed at 840^0C and 850^0C for 6 hours.

The Figure 4.6 indicates resistivity versus temperature graph of Bi(Pb)SrCaCuO thin films annealed at 840^0C and 850^0C for 6 hours. The critical temperatures of the films annealed at 840^0C and 850^0C were found to be about 79 K and 70 K, respectively. Unlike the results of films annealed for 1 hour, 2 and 4 hours, there is a decrease in critical temperature with increasing the annealing temperature. This behaviour may stem from the fabrication conditions.

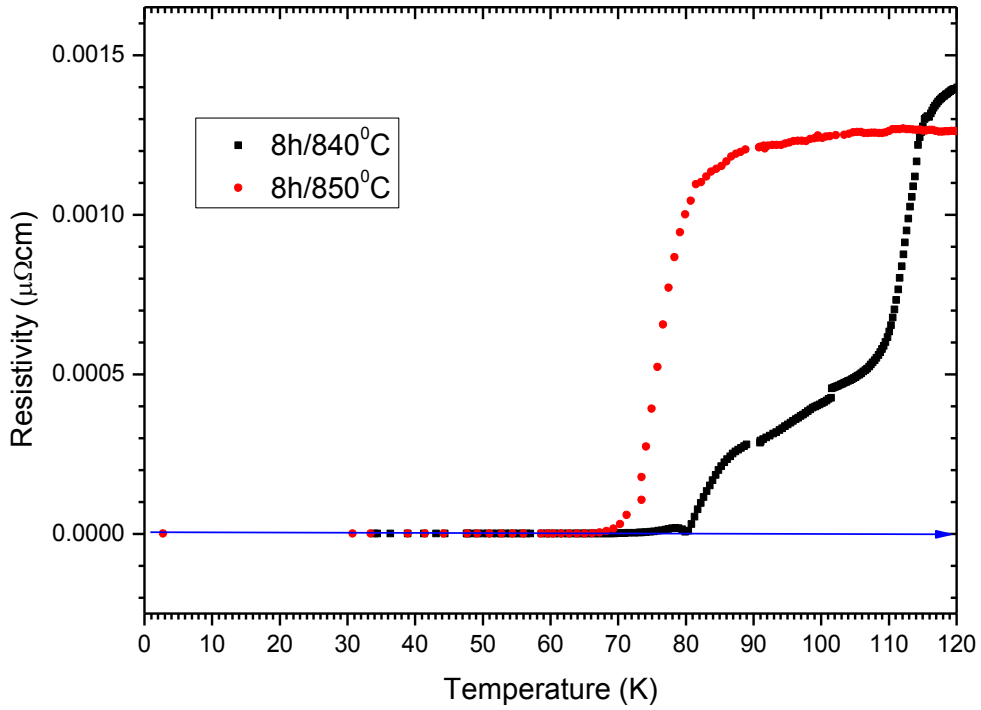

Figure 4.7: Resistivity versus temperature graph of Bi(Pb)SrCaCuO thin films annealed at 840^0C and 850^0C for 8 hours.

Figure 4.7 shows resistivity versus temperature graph of Bi(Pb)SrCaCuO thin films annealed at 840^0C and 850^0C for 8 hours. The critical temperatures of Bi(Pb)SrCaCuO thin films annealed at 840^0C and 850^0C were 81 K and 71 K, respectively. There is a decrease in the critical temperature with increase of the annealing time, which is coincided with the result of the 6 hours annealing time (Figure 4.6). Furthermore, the film annealed at 840^0C has two phases of Bi-2212 and Bi-2223. Both films annealed for 6 and 8 hours were obtained to be very thin in appearance.

4.3 MAGNETORESISTIVITY MEASUREMENTS

Resistivity measurements of the thin film annealed at 840^0C for 2 hours were carried out in various DC magnetic field values (0, 0.5, 1, 3 and 5T) with 1 mA DC current in a cryostat. The magnetic fields were applied to parallel and perpendicular to the thin film surface. The transition temperature T_c^{offset} was noted as the temperature at zero resistivity.

Temperature dependence of resisitivity graphs for the thin film under various magnetic fields which are parallel and perpendicular to the surface are shown in Figures 4.30 and 4.31. Moreover, the values of T_c^{offset} are given at the Table 4.1. It is found that with increasing DC magnetic field T_c^{offset} decreased **[16].** In other words, the decrease in T_c is very prominent for higher external magnetic fields. Moreover, the width increase with increasing external field **[22-23].**

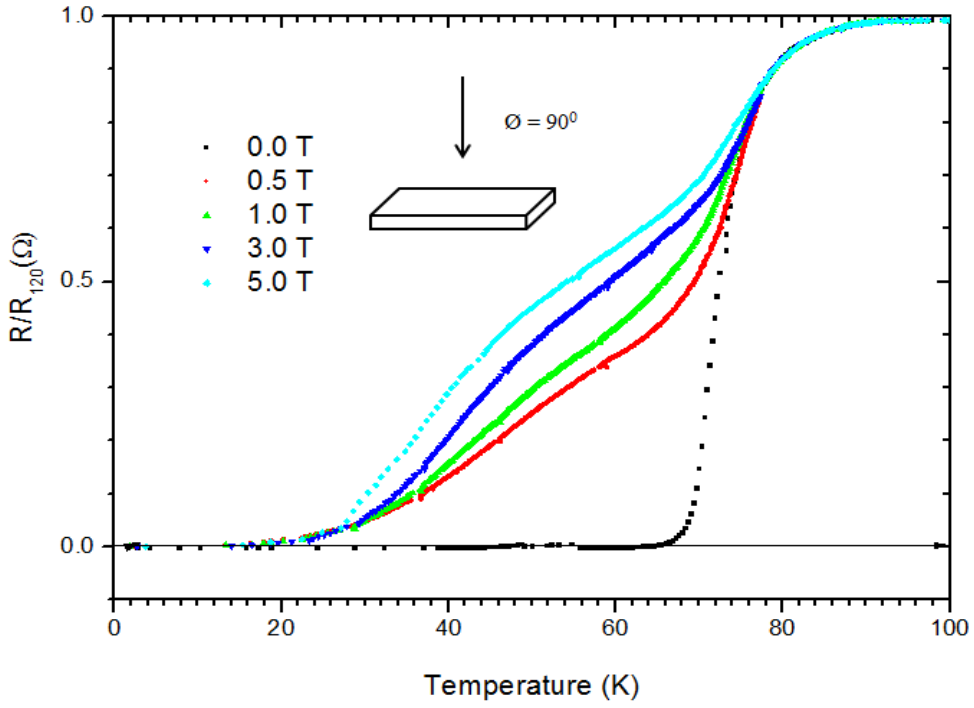

Figure 4.8: Resistance versus temperature graph under various magnetic fields (0, 0.5, 1, 3 and 5T) perpendicular to the film surface (Ø=90^0).

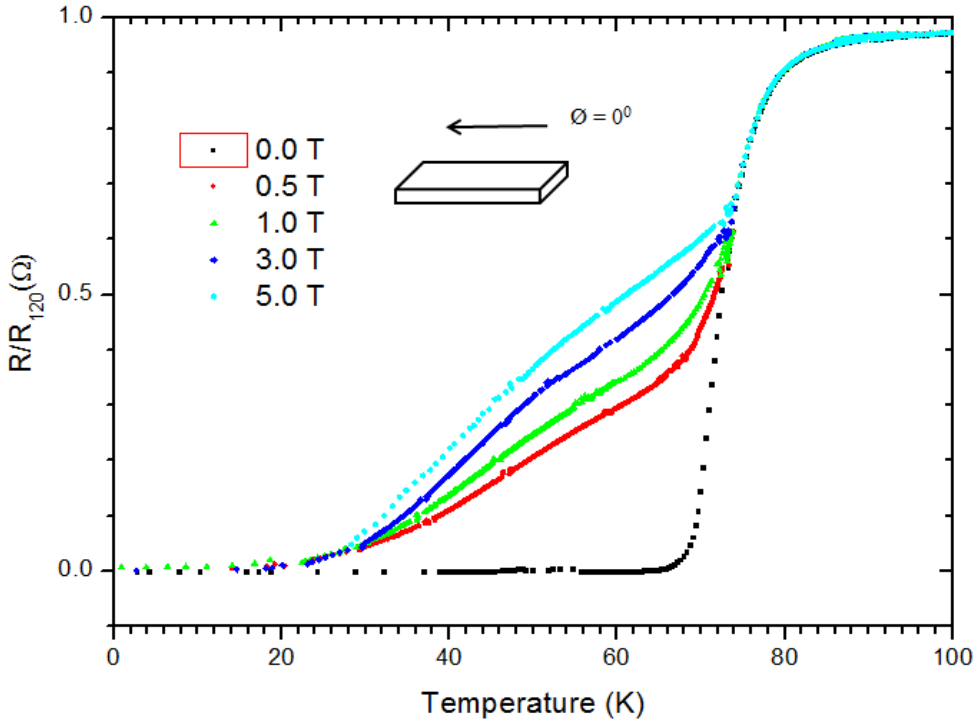

Figure 4.9: Resistance versus temperature graph under various magnetic fields (0, 0.5, 1, 3 and 5T) parallel to the film surface (Ø=0^0).

Applied Magnetic Fields	Critical Temperatures (T_c^{offset})	
	Ø=0^0 to surface of film	**Ø=90^0 to surface of film**
0 T	**69 K**	**69 K**
0.5 T	**40 K**	**36 K**
1 T	**37 K**	**35 K**
3 T	**35 K**	**33 K**
5 T	**32 K**	**29 K**

Table 4.1: The values of critical temperatures of the thin film annealed at 840^0C for 2 hours at applied different magnetic fields and angles.

As shown in Table 4.1, the values of T_c^{offset} for the magnetic field direction at ϕ=0° to the surface of the film are greater than the values of T_c^{offset} for the magnetic field direction at ϕ=90° to the surface of the film. Whereas T_c of the film is noted to be about 40 K for the field applied parallel ($\mu_0 H \perp$ c-axis), it is observed to decrease to 36 K for the field applied perpendicular (μ_0//c-axis) to the surface of the film at 0.5 T. As seen from the results, the effect is more prominent for the field parallel to the c-axis of the film **[22-23].**

4.4 X-RAY DIFFRACTION CHARACTERIZATIONS

The x-ray powder diffraction patterns from the surface of the Bi(Pb)SrCaCuO thin film samples were shown in Figures 4.12 and 4.13. Some of the Miller indices were indicated on these graphs. Lattices parameters were calculated by using the formula of interplanar distances:

$$d^2 = \frac{1}{\frac{h^2}{a^2} + \frac{k^2}{b^2} + \frac{l^2}{c^2}}$$

where *h,k,l* are the Miller indices and *a,b,c* are the lattices parameters of the films **[26]**. Furthermore, the relative volume fractions of the *Bi-2223* and *Bi-2212* phases were calculated from the peak intensities of the same particular peaks, using the following expressions **[18, 19];**

$$f_{(2223)} = \frac{\sum I_{H(hkl)}}{\sum I_{H(hkl)} + \sum I_{L(hkl)}}$$

$$f_{(2212)} = \frac{\sum I_{L(hkl)}}{\sum I_{H(hkl)} + \sum I_{L(hkl)}}$$

$I_{H(hkl)}$ and $I_{L(hkl)}$ are the intensities of the *(hkl)* diffraction lines for *Bi-2223* and *Bi-2212* phases, respectively. The determined relative volume fractions and lattices parameters of the samples are listed in Table 4.2 **[24].**

Samples	**Lattice Parameter a (Å)**	**Lattice Parameter c (Å)**	**Volume Fractions (%)**	
			2212	**2223**
840^0C - 1 hour	5.437	30.9946	75	25
840^0C - 2 hours	5.342	30.3954	85	15
840^0C - 4 hours	5.401	30.5583	77	23
840^0C - 6 hours	5.361	30.4970	60	40
840^0C - 8 hours	5.370	30.7853	52	48
850^0C - 1 hour	5.411	30.8687	73	27
850^0C - 2 hours	5.521	30.6817	77	23
850^0C - 4 hours	5.443	30.9946	79	21
850^0C - 6 hours	5.411	30.8061	85	15
850^0C - 8 hours	5.401	30.5993	81	19

Table 4.2: Lattice parameter *a*, and *c*, and volume fractions of and Bi(Pb)SrCaCuO thin film samples annealed at 840^0C and 850^0C.

It is known that when Bi-2223 volume fraction increases, T_c also increases. This relation was proved in our results. Based on the calculations, Bi-2223 phase was found to be dominant on the film annealed for 8 hours. The samples consist of 2212 as the major phase and 2223 as the minor phase **[25].** Moreover, it is seen that the values of calculated lattices parameters are close to their theoretical values.

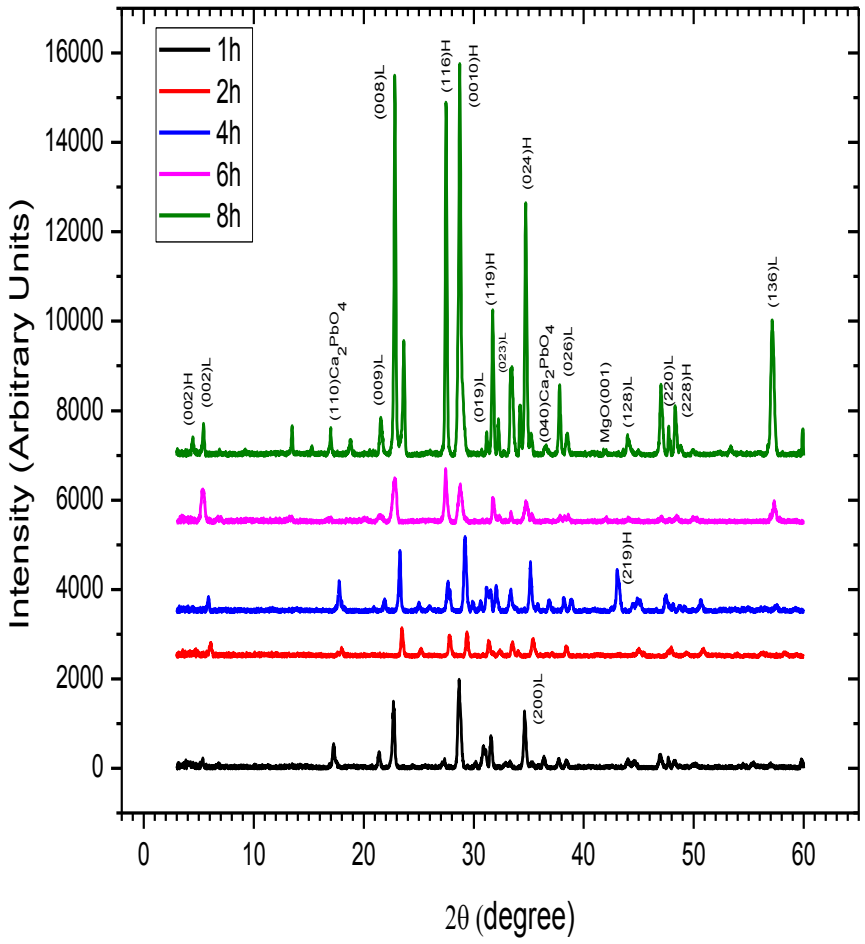

Figure 4.10: XRD patterns from the surface of the Bi(Pb)SrCaCuO thin film samples annealed at 840^0C.

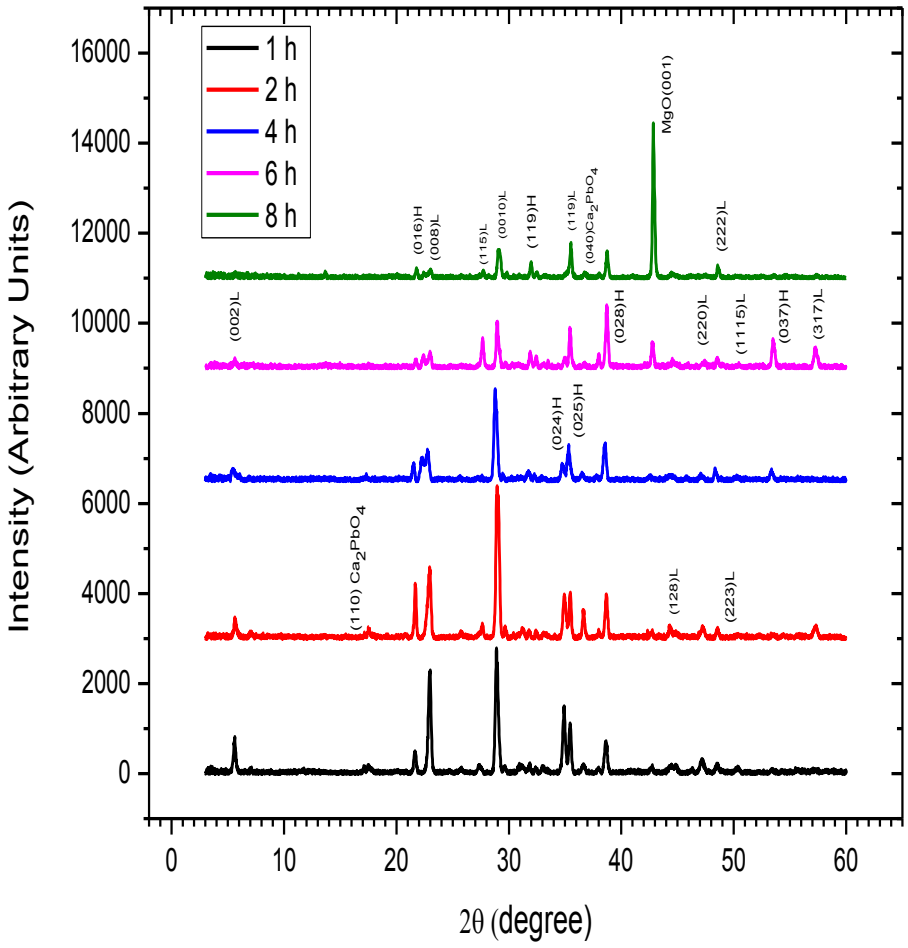

Figure 4.11: XRD patterns from the surface of the Bi(Pb)SrCaCuO thin film samples annealed at 850^0C.

4.5 SCANNING ELECTRON MICROSCOPY INVESTIGATIONS

The structure of surface morphology of the Bi(Pb)SrCaCuO thin film samples were investigated by scanning electron microscopy (SEM) in order to determine the grain size and possible precipitation at the grain boundaries.

SEM micrographs for all the samples were shown in Figure 4.10 (a-b), 4.11 (a-b), 4.12 (a-b) 4.13 (a-b) and 4.14 (a-b), which indicate the surface micrographs for the thin films annealed at 840^0C for 1, 2 4, 6 and 8 hours, respectively. Needle-like and flake-like grains were observed in the films produced in this work. When the SEM photos of the thin films annealed at 840^0C were compered with each other the film annealed for 8 hours, surface of which was observed to be more smoother and denser, was found to obtain almost no dislocations between the grains. This behaviour is similar to that of other researcher's result**.** Moreover, the grain size of the film annealed for 4 hours is obtained to be relatively greater than the other samples **[16].**

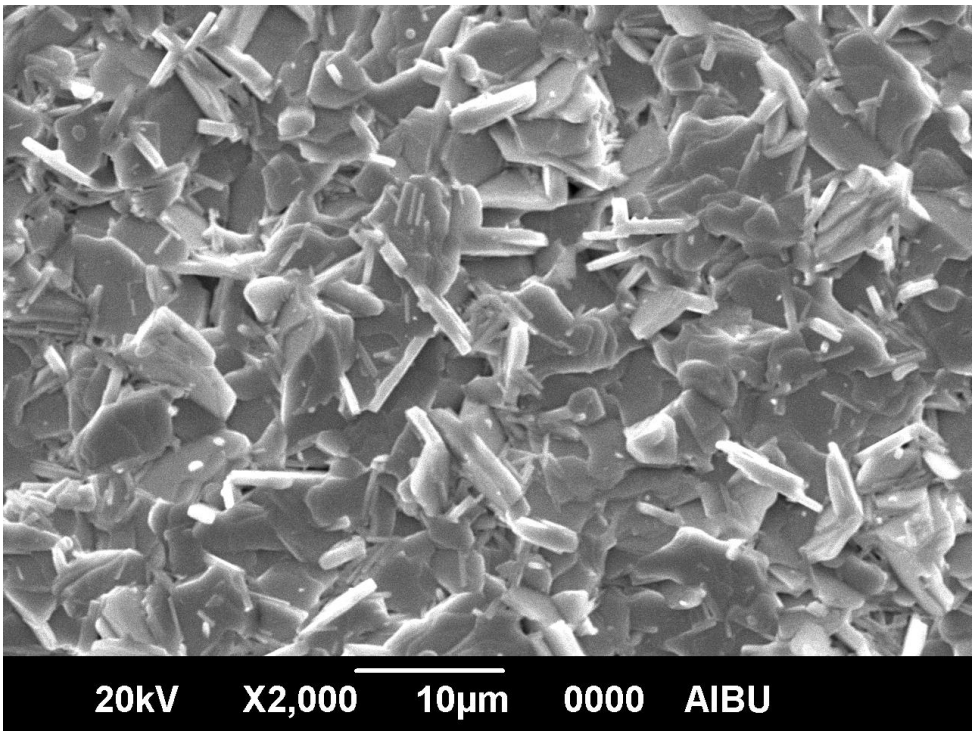

(a)

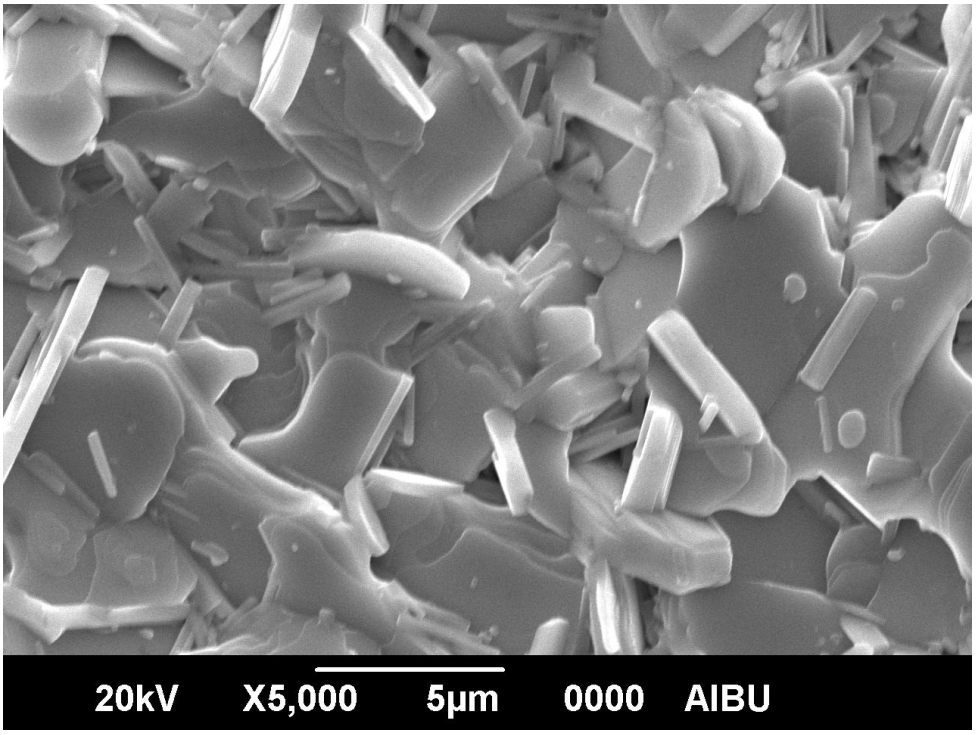

(b)

Figure 4.12 a-b: SEM micrographs of thin film at 840^0C for 1 hour.

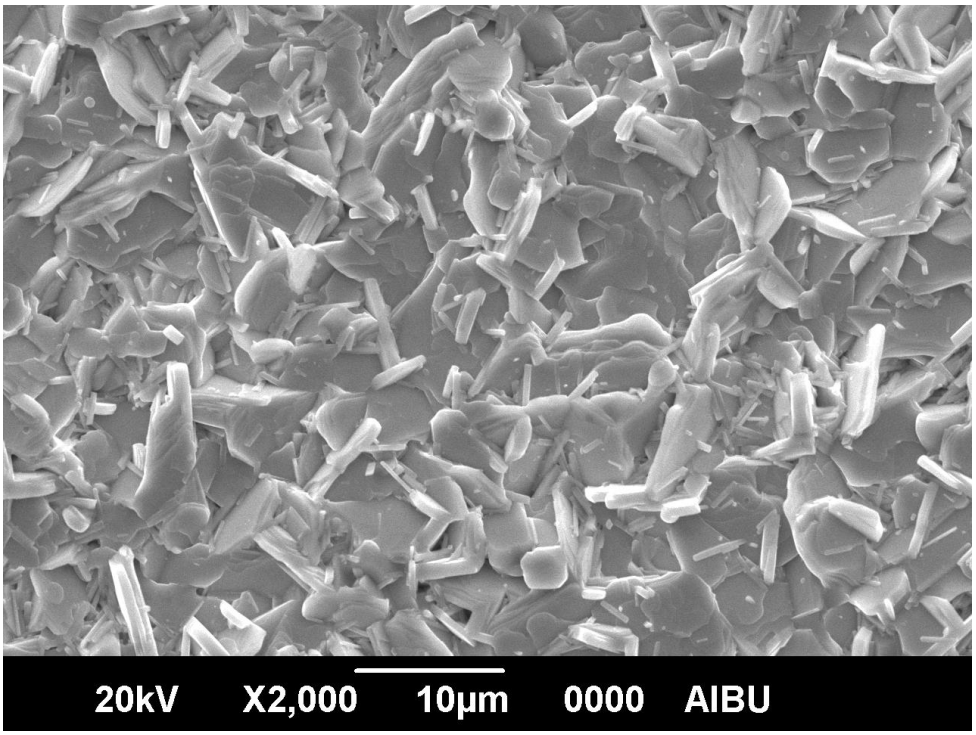

(a)

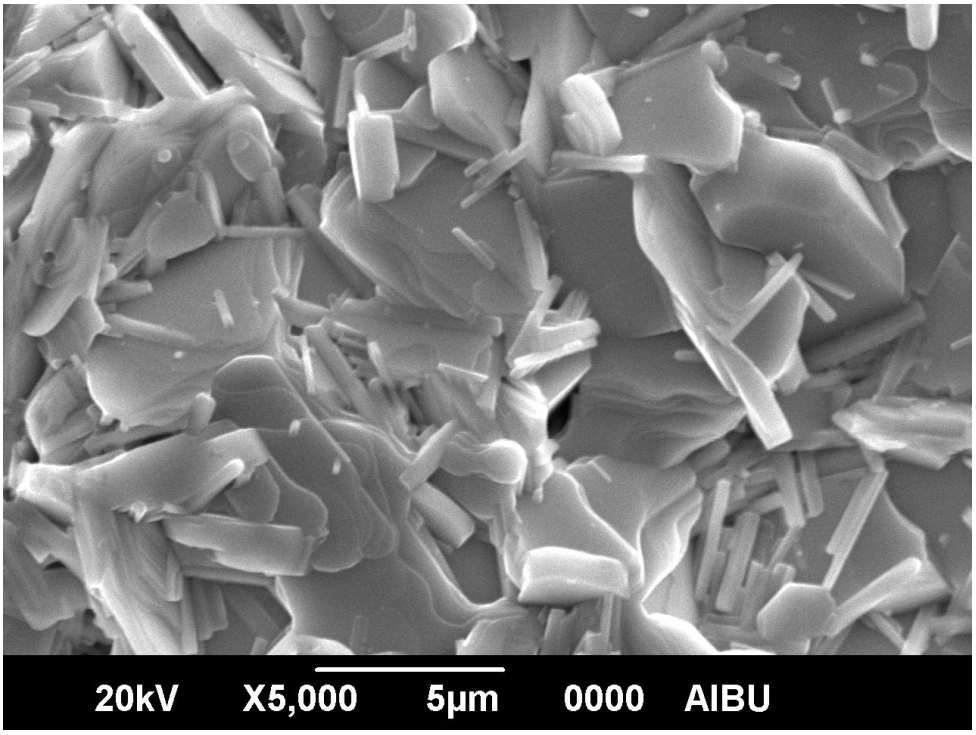

(b)

Figure 4.13 a-b: SEM micrographs of thin film at 840^0C for 2 hours.

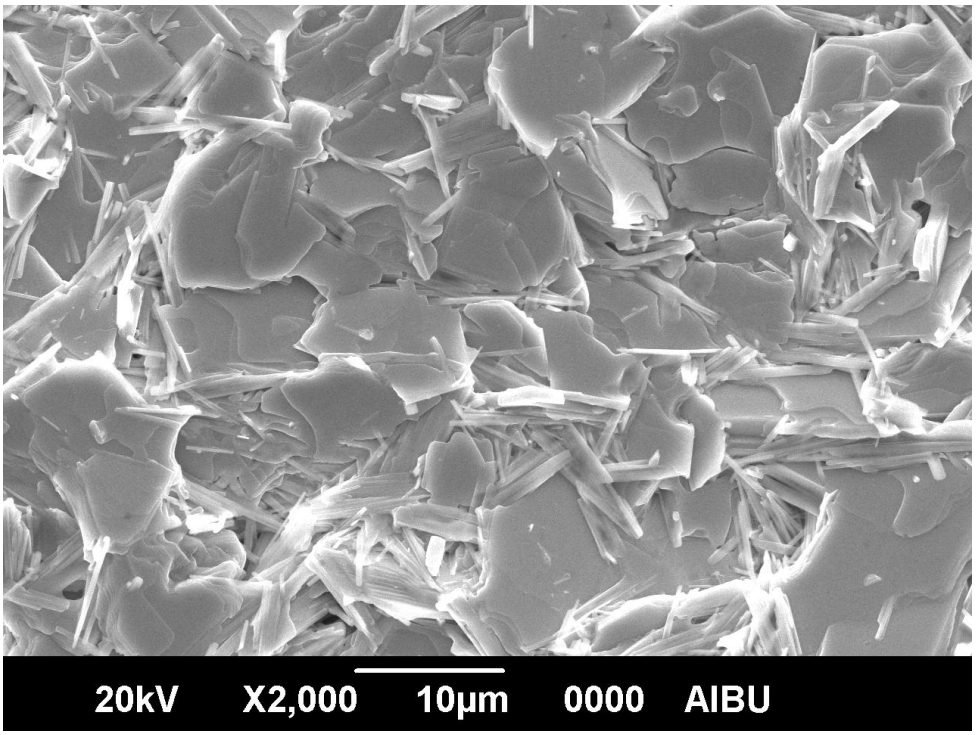

(a)

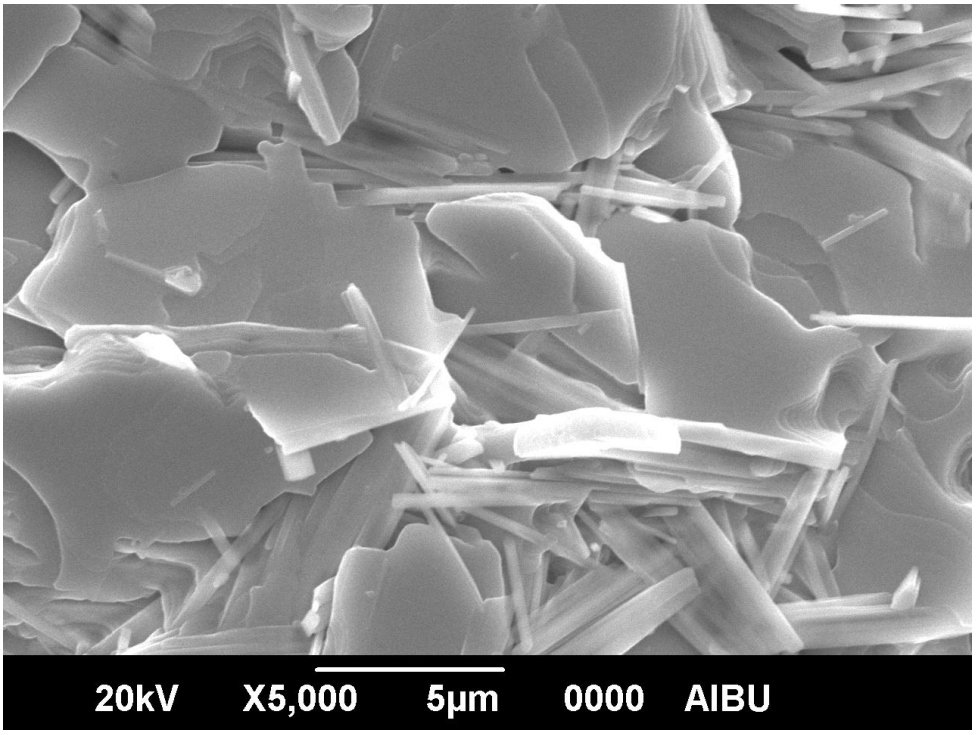

(b)

Figure 4.14 a-b: SEM micrographs of thin film at 840^0C for 4 hours.

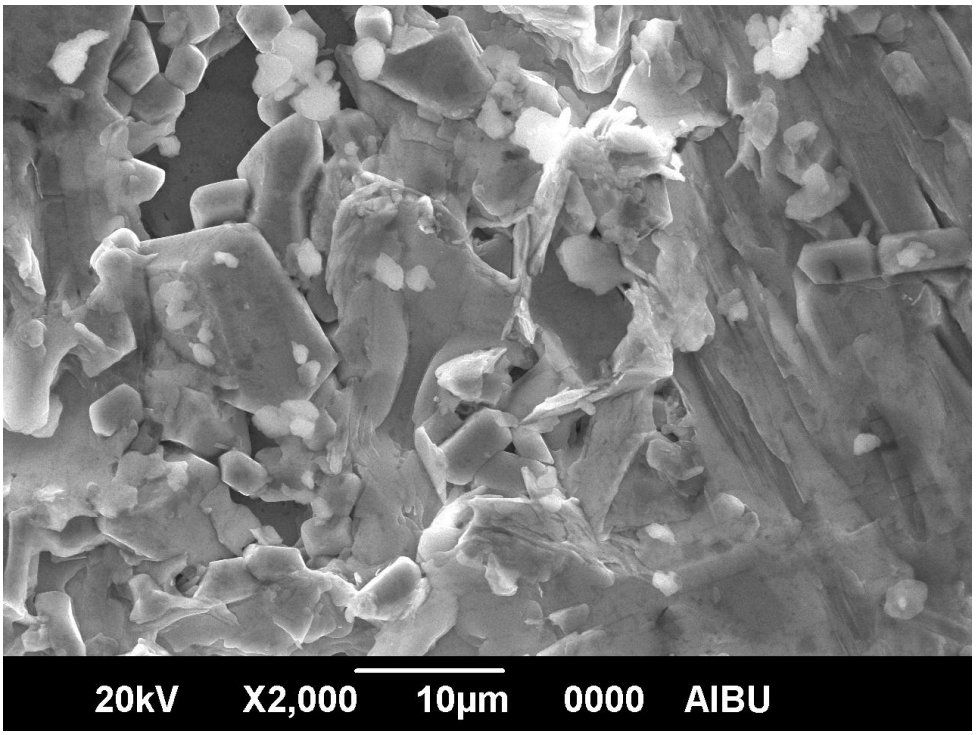

(a)

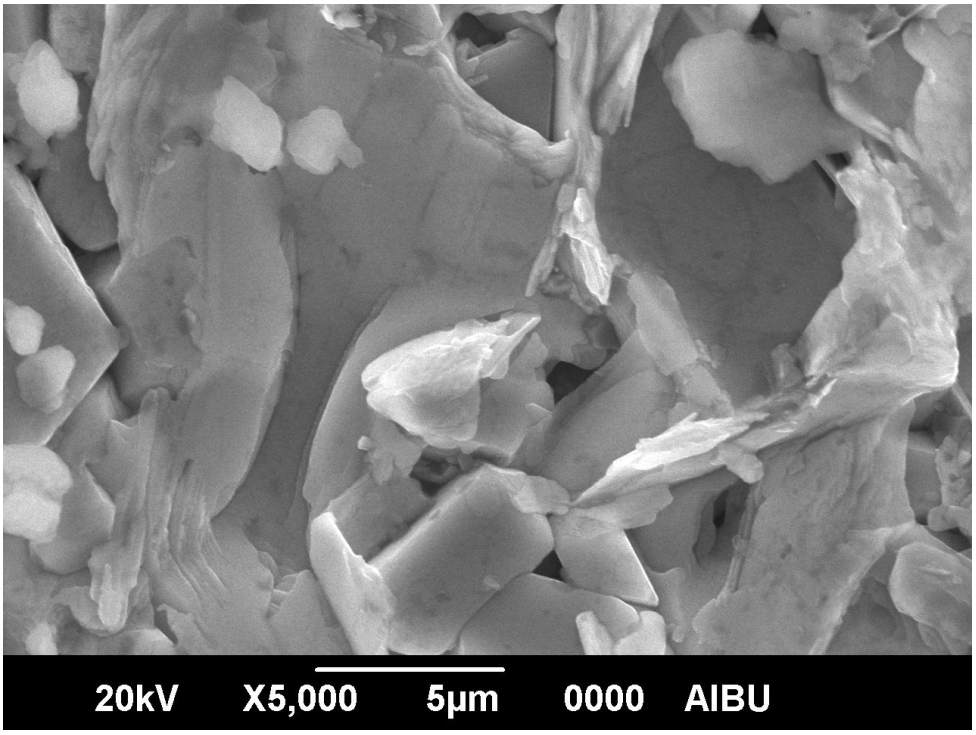

(b)

Figure 4.15 a-b: SEM micrographs of thin film at 840^0C for 6 hours.

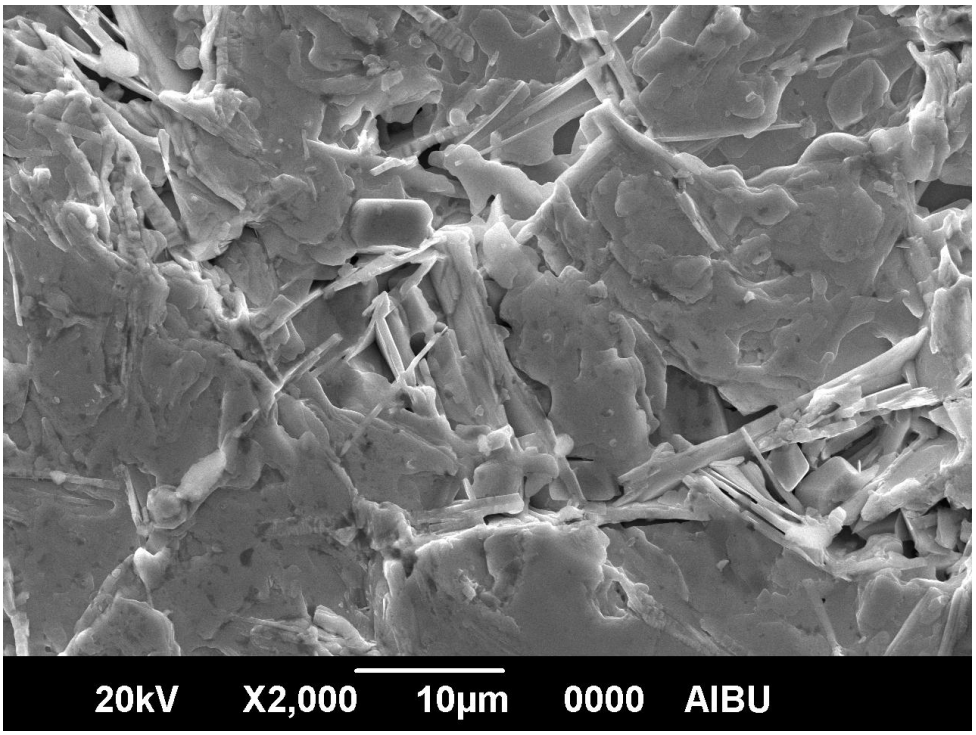

(a)

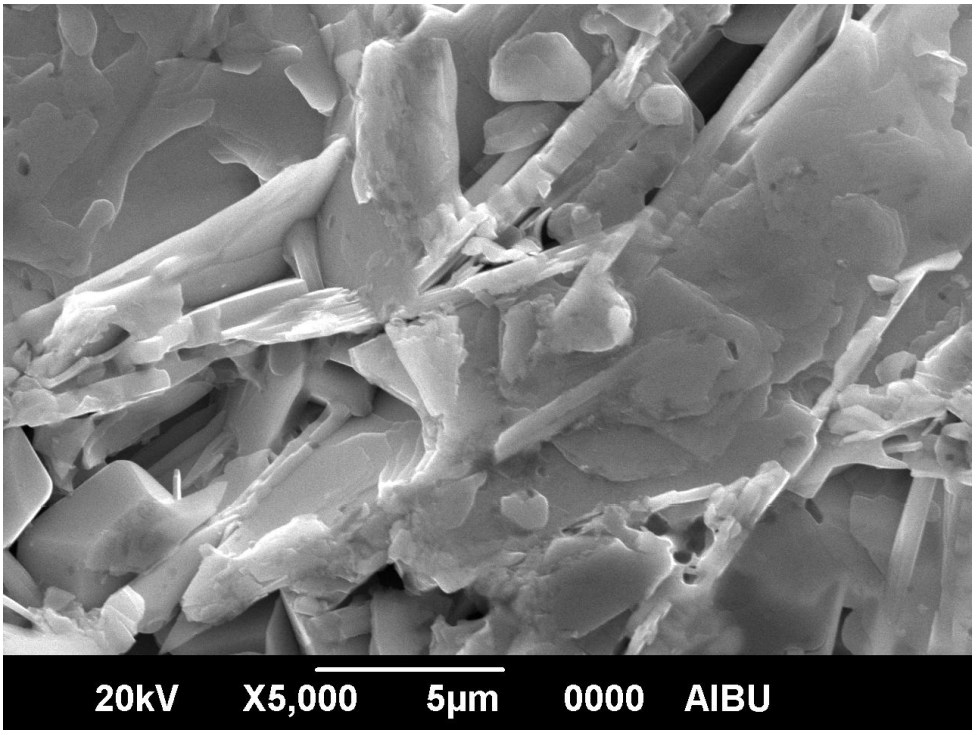

(b)

Figure 4.16 a-b: SEM micrographs of thin film at 840^0C for 8 hours.

Moreover, the surface micrographes for the Bi(Pb)SrCaCuO thin films annealed at 850^0C were given figure 4.15 (a-b), 4.16 (a-b), 4.17 (a-b), 4.18 (a-b) and 4.19 (a-b). Some needle-like grains were obviously seen at the films annealed for 2 and 6 hours. But, there were voids in the samples while the surface of the films annealed at 840^0C were smoother and denser. These results show that the surface morphology of the sample is worsened with increase in annealing temperature from 840^0C to 850^0C **[17].**

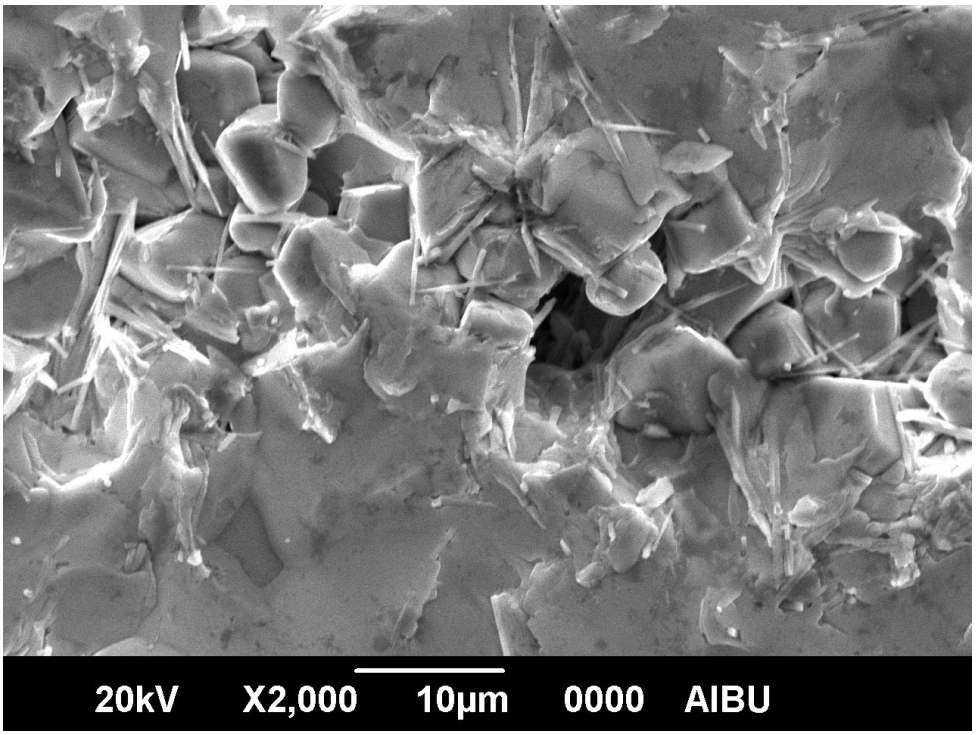

(a)

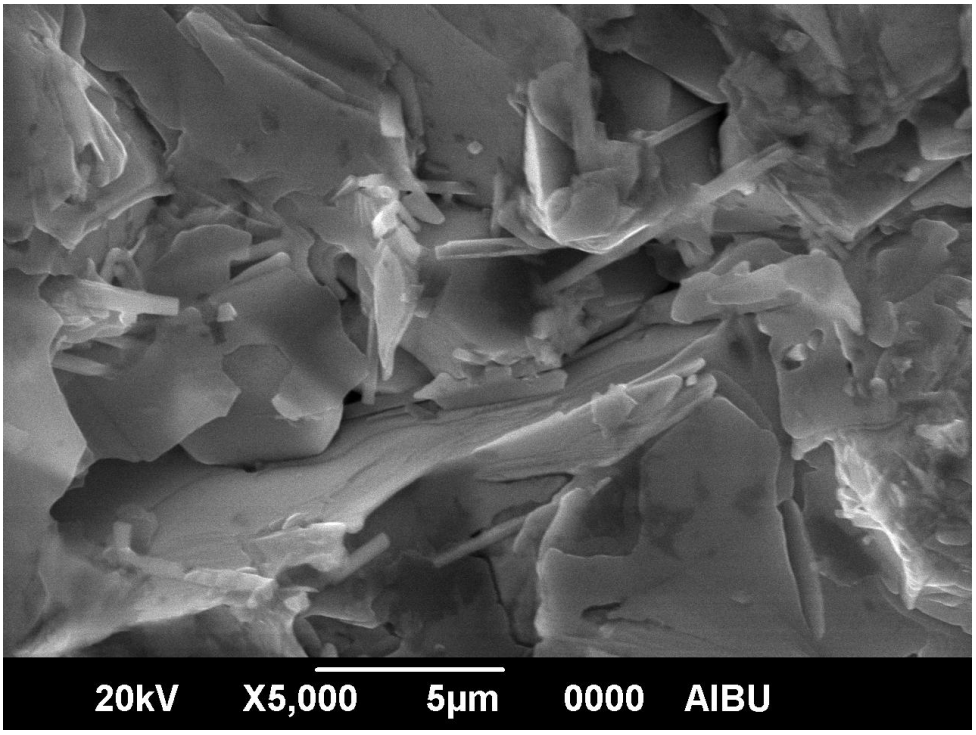

(b)

Figure 4.17 a-b: SEM micrographs of thin film at 850^0C for 1 hour.

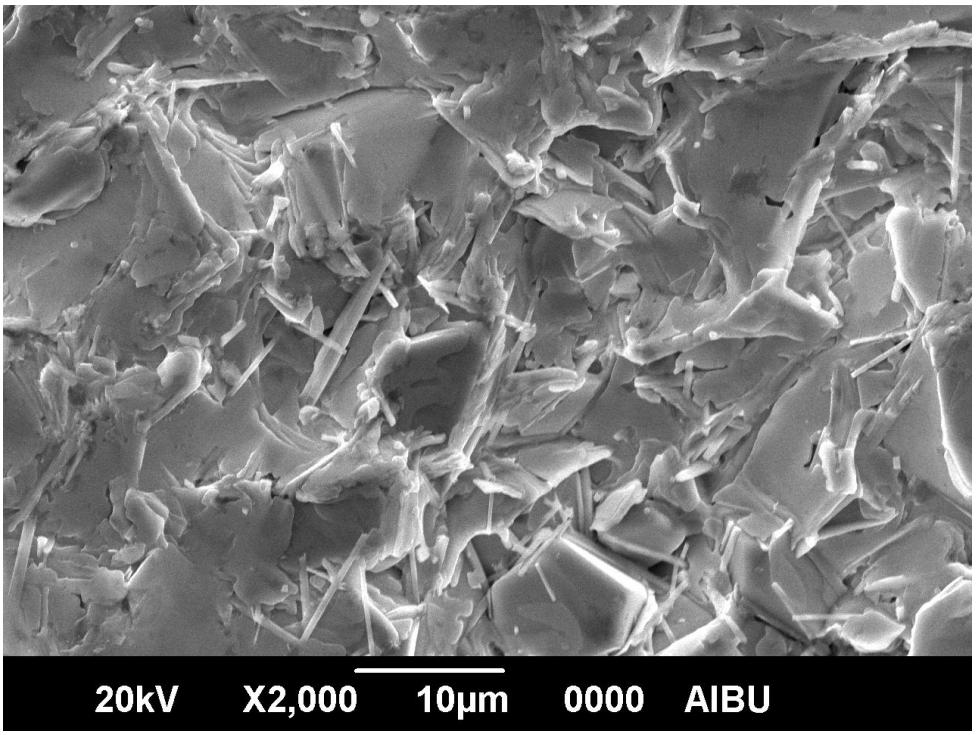

(a)

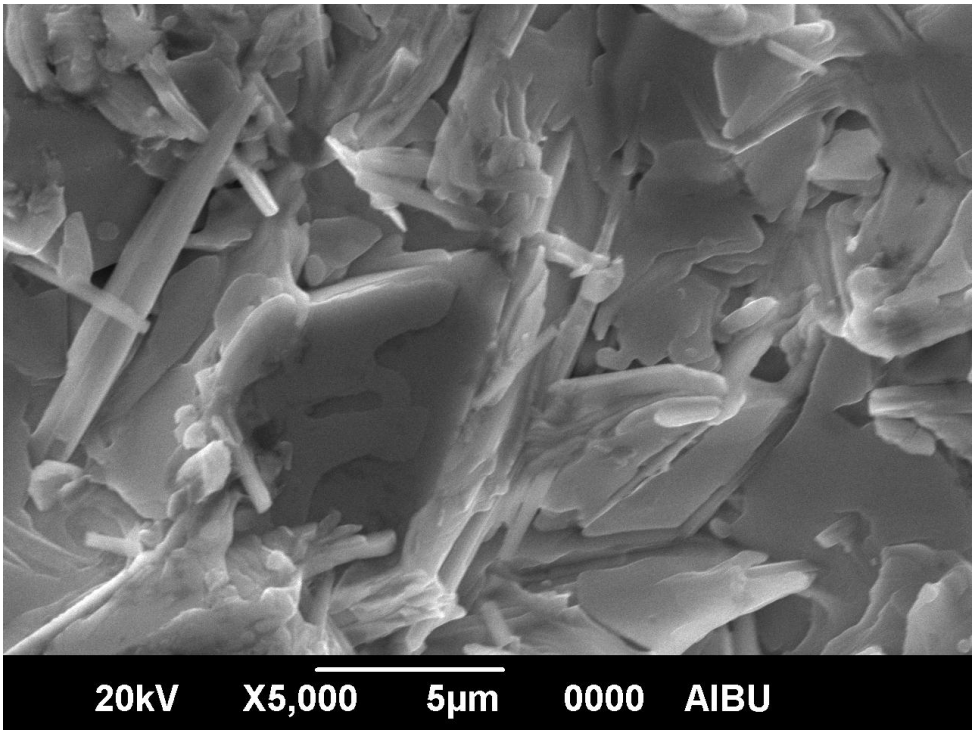

(b)

Figure 4.18 a-b: SEM micrographs of thin film at 850^0C for 2 hours.

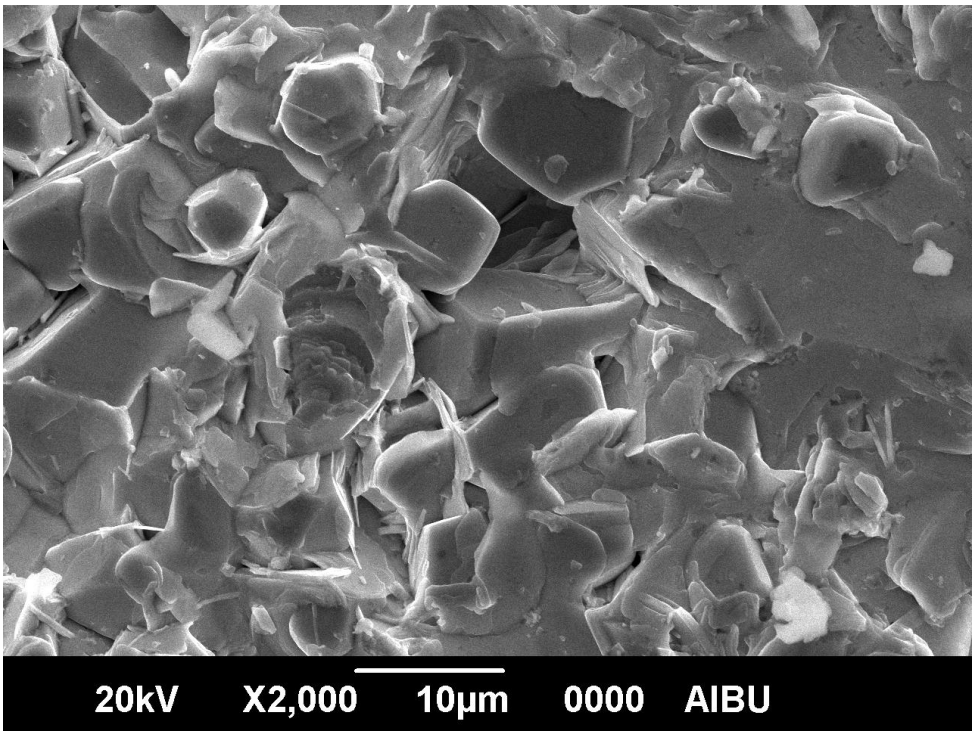

(a)

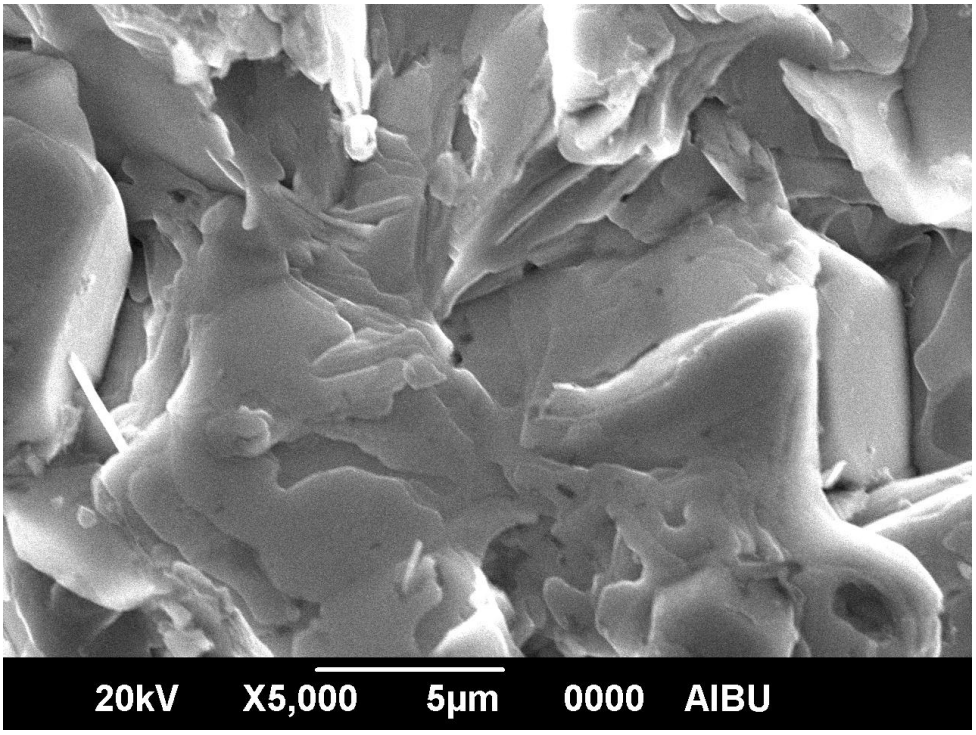

(b)

Figure 4.19 a-b: SEM micrographs of thin film at 850^0C for 4 hours.

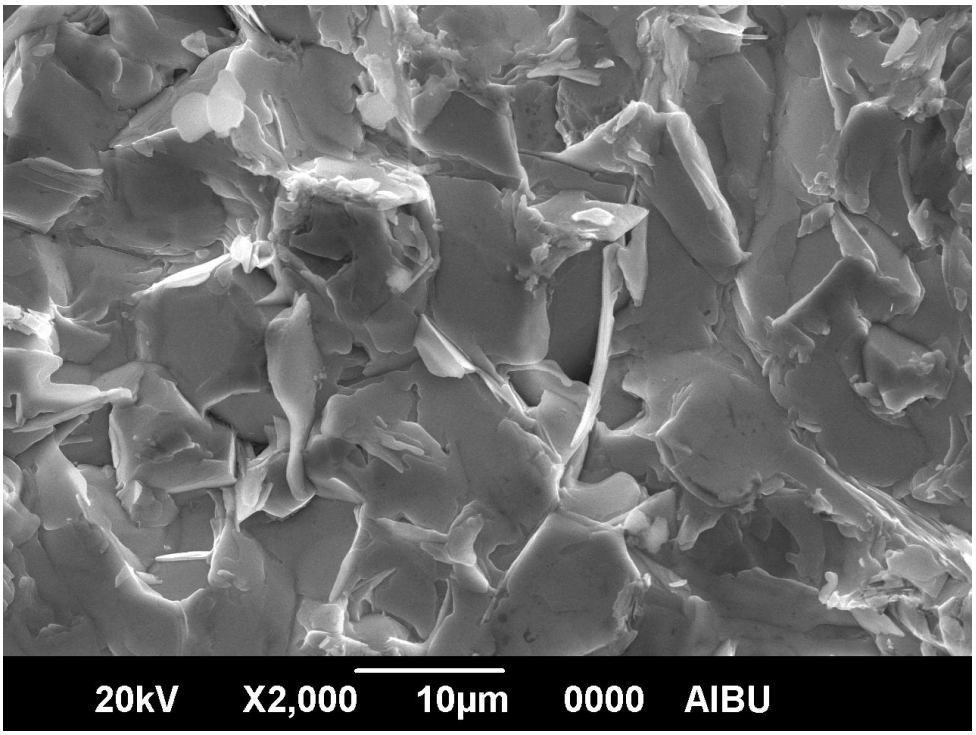

(a)

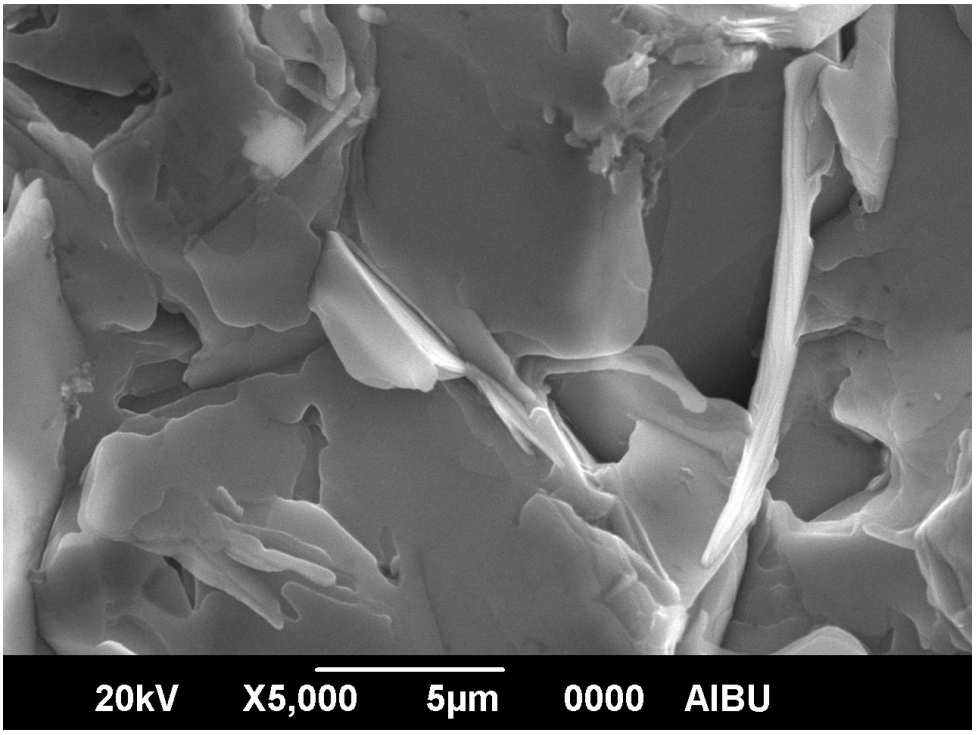

(b)

Figure 4.20 a-b: SEM micrographs of thin film at 850^0C for 6 hours.

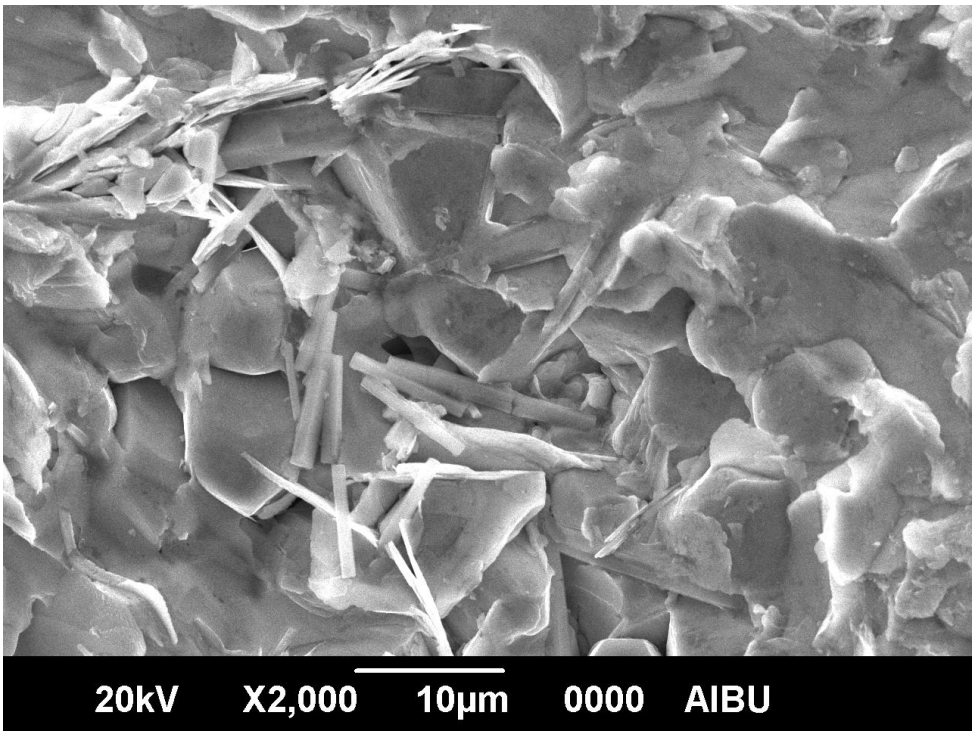

(a)

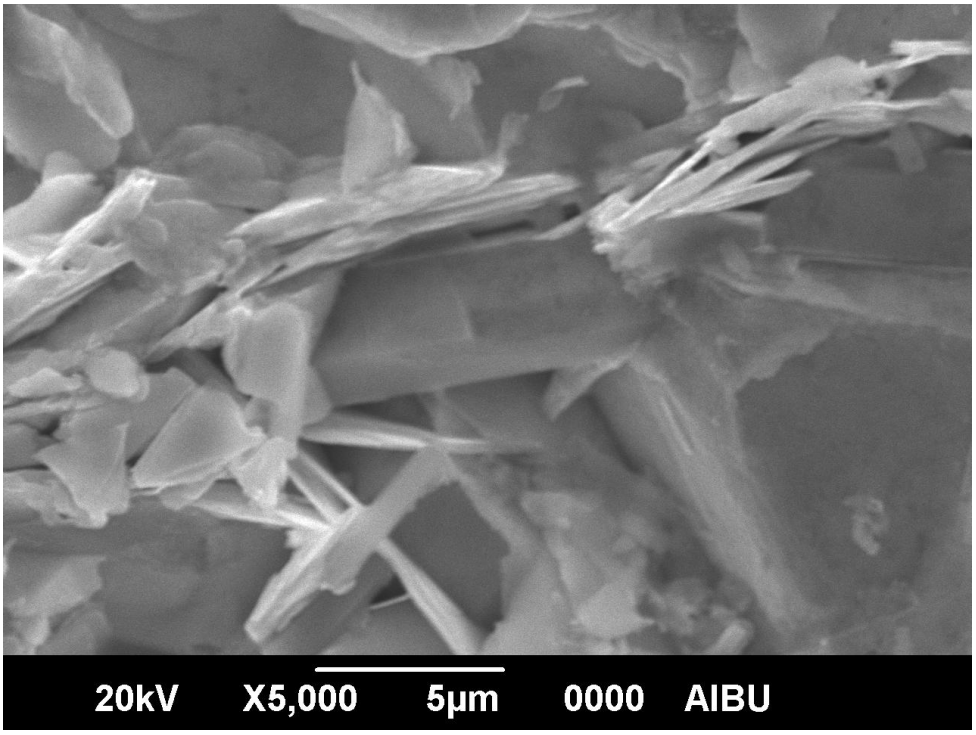

(b)

Figure 4.21 a-b: SEM micrographs of thin film at 850^0C for 8 hours.

4.6 ENERGY DISPERSIVE SPECTRUM ANALYSIS

In this section, energy dispersive spectrum (EDS) analysis of Bi(Pb)SrCaCuO thin films annealed at 840^0C and 850^0C for several hours were given below (Figures 4.20, 4.21, 4.22, 4.23, 4.24, 4.25, 4.26, 4.27, 4.28 and 4.29). In addition, the weight percent of elements of Bi(Pb)SrCaCuO thin films were theoretically calculated. The theoretical values of weight percent of elements of Bi(Pb)SrCaCuO thin films were compared with their experimental values (Tables 4.1, 4.2, 4.3, 4.4, 4.5, 4.6, 4.7, 4.8, 4.9 and 4.10).

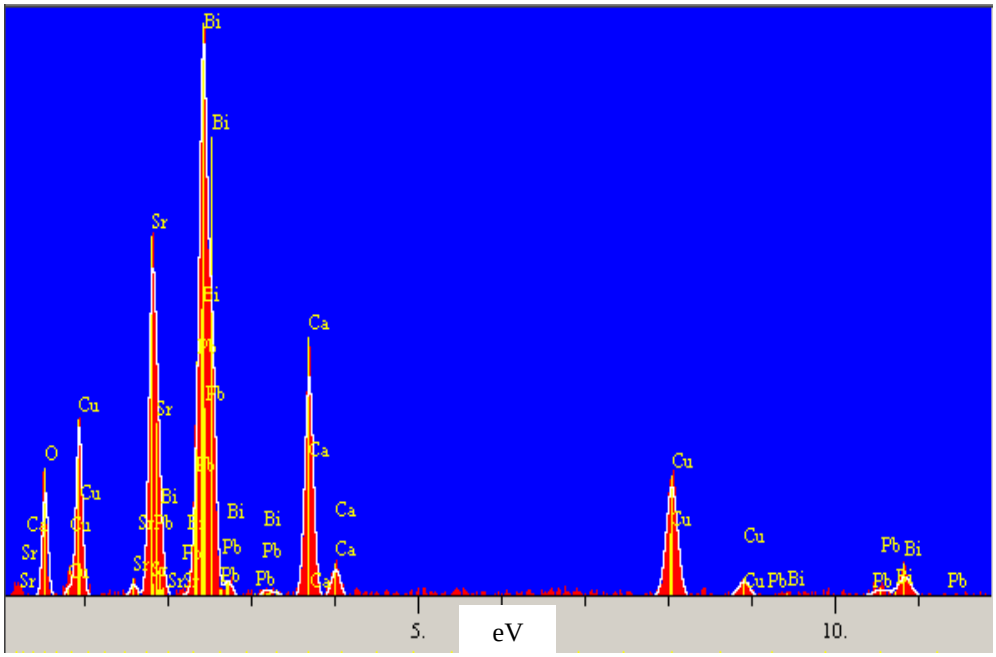

Figure 4.22: Energy dispersive spectrum analysis of Bi(Pb)SrCaCuO thin film fabricated at 840^0C for 1 hour.

Elt.	Line	Intensity (film) (c/s)	Error 2-sig	EDS (film)	Units	Target	Difference between target and results of EDS (%)
O	Ka	15.42	1.111	10.02	wt.%	13.73	-3.710
Ca	Ka	48.61	1.972	7.971	wt.%	5.50	+2.471
Cu	Ka	33.07	1.626	12.986	wt.%	12.00	+0.986
Sr	La	51.27	2.025	20.836	wt.%	15.05	+5.786
Pb	La	2.72	0.467	10.459	wt.%	17.79	-7.331
Bi	La	7.03	0.750	30.542	wt.%	35.90	-5.358
TOTAL				100.000	wt.%	100.00	

Table 4.3: Experimental and theoretical values of weight percent of $Bi_2Pb_1Sr_2Ca_{1.6}Cu_{2.2}O_8$ thin film fabricated at 840^0C for 1 hour.

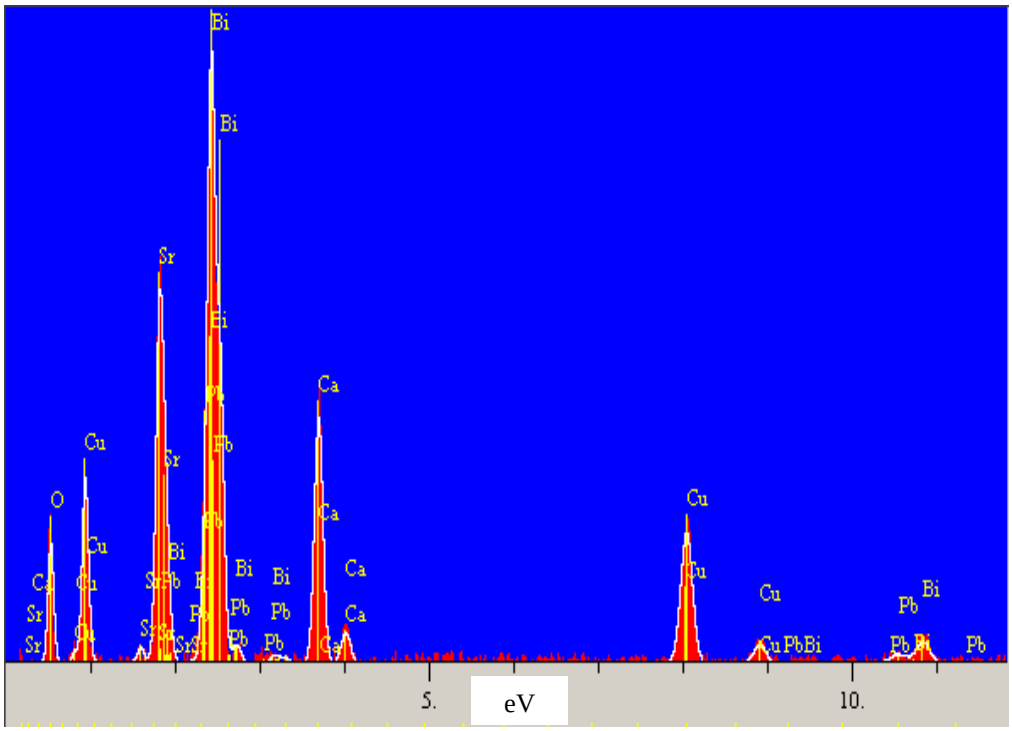

Figure 4.23: Energy dispersive spectrum analysis of Bi(Pb)SrCaCuO thin film fabricated at 840^0C for 2 hours.

Elt.	Line	Intensity (c/s)	Error 2-sig	EDS (Film)	Units	Target	Difference between target and results of EDS (%)
O	Ka	15.79	1.124	10.19	wt.%	13.73	-3.540
Ca	Ka	48.50	1.970	7.912	wt.%	5.50	+2.412
Cu	Ka	34.91	1.671	13.679	wt.%	12.00	+1.679
Sr	La	51.95	2.039	21.105	wt.%	15.05	+6.055
Pb	La	2.79	0.472	10.704	wt.%	17.79	-7.086
Bi	La	6.70	0.732	29.110	wt.%	35.90	-6.790
TOTAL				100.00	wt.%	100.00	

Table 4.4: Experimental and theoretical values of weight percent of $Bi_2Pb_1Sr_2Ca_{1.6}Cu_{2.2}O_8$ thin film fabricated at 840^0C for 2 hours.

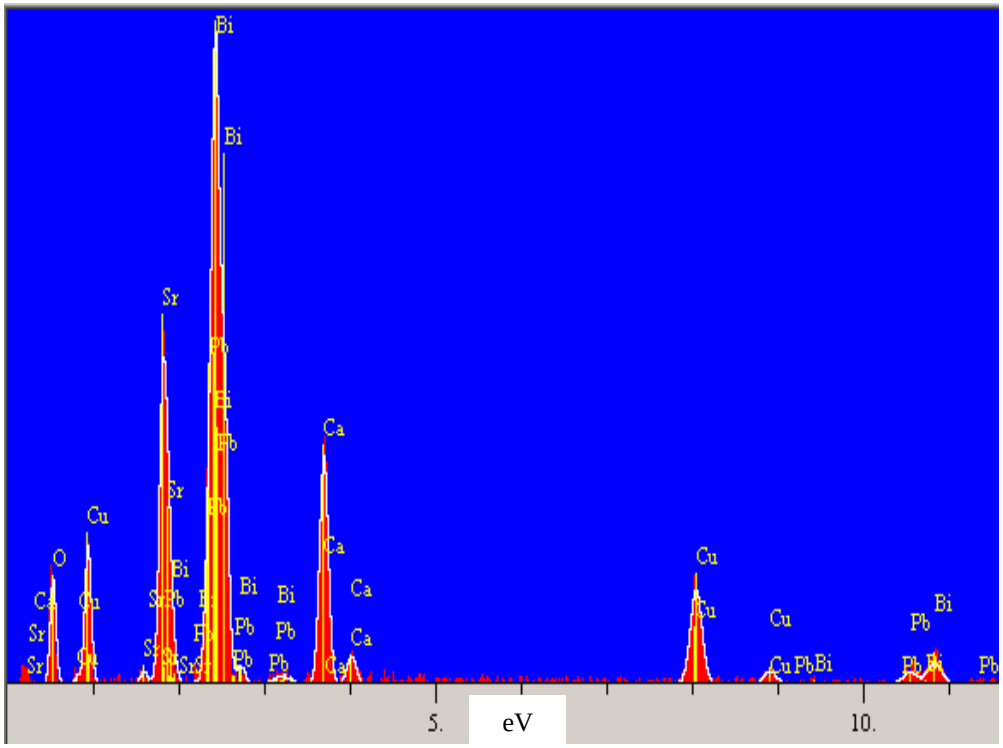

Figure 4.24: Energy dispersive spectrum analysis of Bi(Pb)SrCaCuO thin film fabricated at 840^0C for 4 hours.

Elt.	Line	Intensity (c/s)	Error 2-sig	EDS (Film)	Units	Target	Difference between target and results of EDS (%)
O	Ka	14.12	1.063	9.53	wt.%	13.73	-4.200
Ca	Ka	45.85	1.915	7.858	wt.%	5.50	+2.358
Cu	Ka	25.35	1.424	10.243	wt.%	12.00	-1.757
Sr	La	46.19	1.922	19.190	wt.%	15.05	+4.140
Pb	La	3.85	0.555	15.131	wt.%	17.79	-2.659
Bi	La	7.02	0.749	31.209	wt.%	35.90	-4.691
TOTAL				100.000	wt.%	100.00	

Table 4.5: Experimental and theoretical values of weight percent of $Bi_2Pb_1Sr_2Ca_{1.6}Cu_{2.2}O_8$ thin film fabricated at 840^0C for 4 hours.

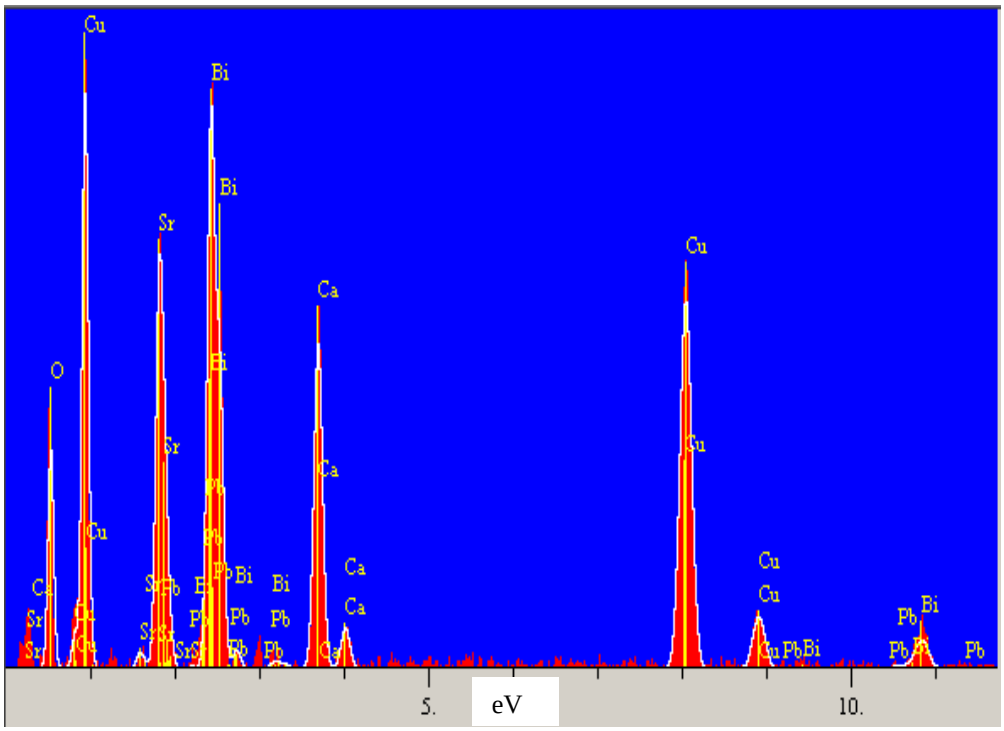

Figure 4.25: Energy dispersive spectrum analysis of Bi(Pb)SrCaCuO thin film fabricated at 840^0C for 6 hours.

Elt.	Line	Intensity (c/s)	Error 2-sig	EDS (Film)	Units	Target	Difference between target and results of EDS (%)
O	Ka	23.04	1.358	11.55	wt.%	13.73	-2.180
Ca	Ka	50.79	2.016	6.838	wt.%	5.50	+1.338
Cu	Ka	77.80	2.495	26.310	wt.%	12.00	+14.310
Sr	La	46.08	1.920	17.237	wt.%	15.05	+2.187
Pb	La	0.77	0.248	2.592	wt.%	17.79	-15.198
Bi	La	7.10	0.754	27.187	wt.%	35.90	-8.713
TOTAL				100.000	wt.%	100.00	

Table 4.6: Experimental and theoretical values of weight percent of $Bi_2Pb_1Sr_2Ca_{1.6}Cu_{2.2}O_8$ thin film fabricated at 840^0C for 6 hours.

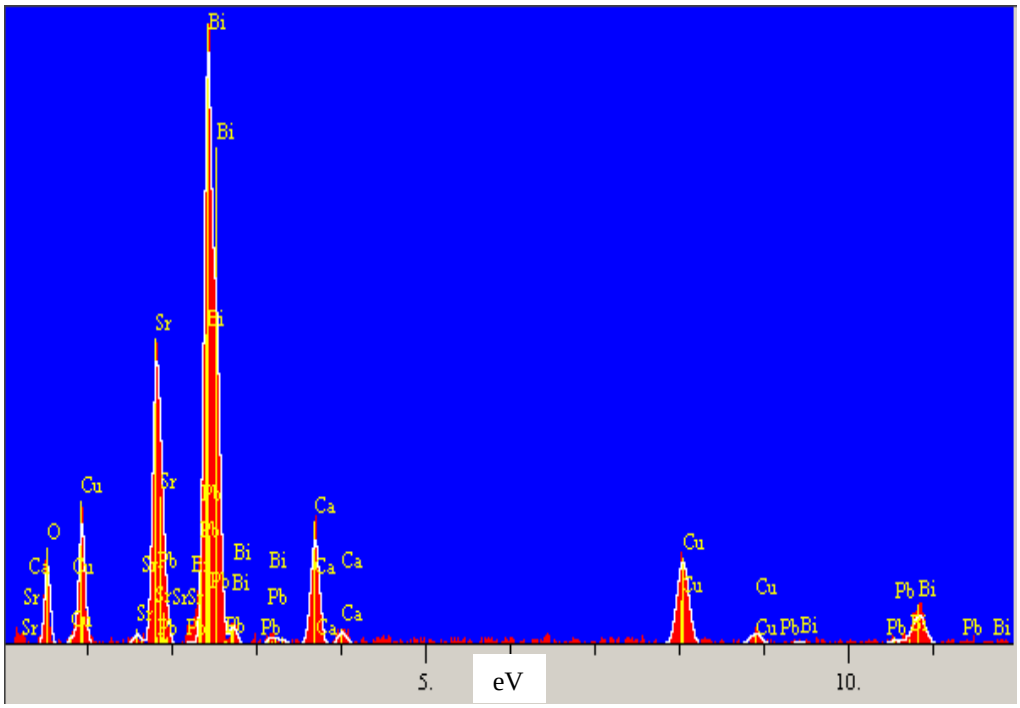

Figure 4.26: Energy dispersive spectrum analysis of Bi(Pb)SrCaCuO thin film fabricated at 840^0C for 8 hours.

Elt.	Line	Intensity (c/s)	Error 2-sig	EDS (Film)	Units	Target	Difference between target and results of EDS (%)
O	Ka	12.62	1.005	7.80	wt.%	13.73	-5.930
Ca	Ka	25.41	1.426	4.167	wt.%	5.50	-1.333
Cu	Ka	27.30	1.478	10.328	wt.%	12.00	-1.672
Sr	La	48.41	1.968	19.372	wt.%	15.05	+4.322
Pb	La	1.62	0.360	5.906	wt.%	17.79	-11.884
Bi	La	11.34	0.952	46.833	wt.%	35.90	+10.933
TOTAL				100.000	wt.%	100.00	

Table 4.7: Experimental and theoretical values of weight percent of $Bi_2Pb_1Sr_2Ca_{1.6}Cu_{2.2}O_8$ thin film fabricated at 840^0C for 8 hours.

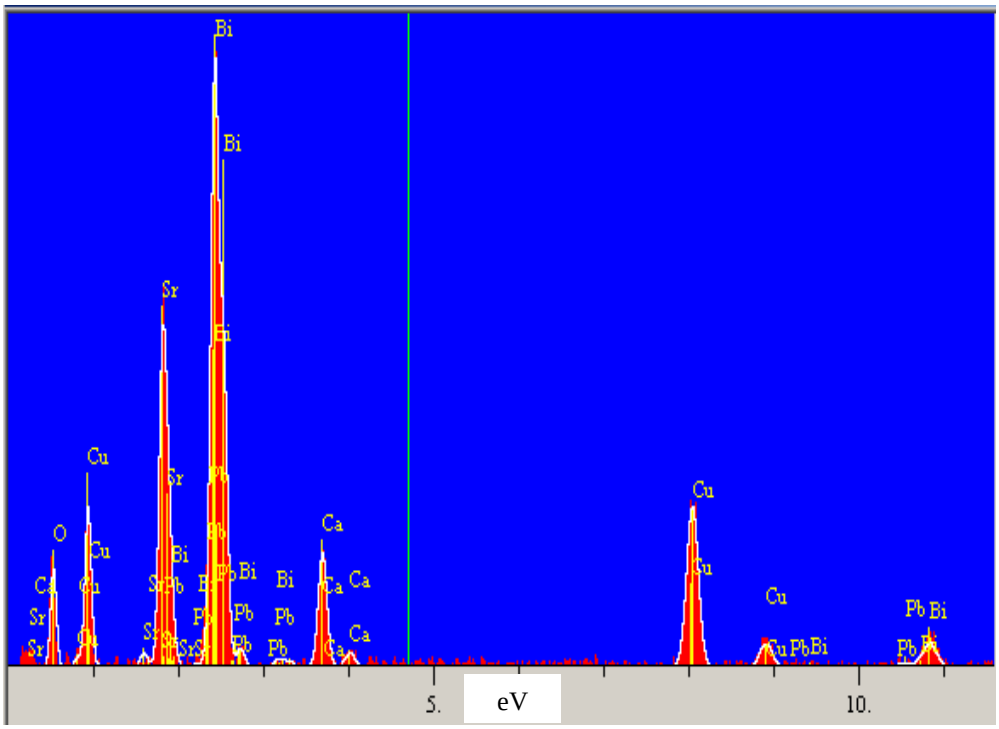

Figure 4.27: Energy dispersive spectrum analysis of Bi(Pb)SrCaCuO thin film fabricated at 850^0C for 1 hour.

Elt.	Line	Intensity (c/s)	Error 2-sig	EDS (Film)	Units	Target	Difference between target and results of EDS (%)
O	Ka	12.78	1.011	8.68	wt.%	13.73	-5.050
Ca	Ka	22.38	1.338	4.069	wt.%	5.50	-1.431
Cu	Ka	42.59	1.846	18.421	wt.%	12.00	+6.421
Sr	La	47.59	1.951	22.291	wt.%	15.05	+7.241
Pb	La	1.24	0.315	5.246	wt.%	17.79	-12.554
Bi	La	7.32	0.765	35.070	wt.%	35.90	-0.830
TOTAL				100.000	wt.%	100.00	

Table 4.8: Experimental and theoretical values of weight percent of $Bi_2Pb_1Sr_2Ca_{1.6}Cu_{2.2}O_8$ thin film fabricated at 850^0C for 1 hour.

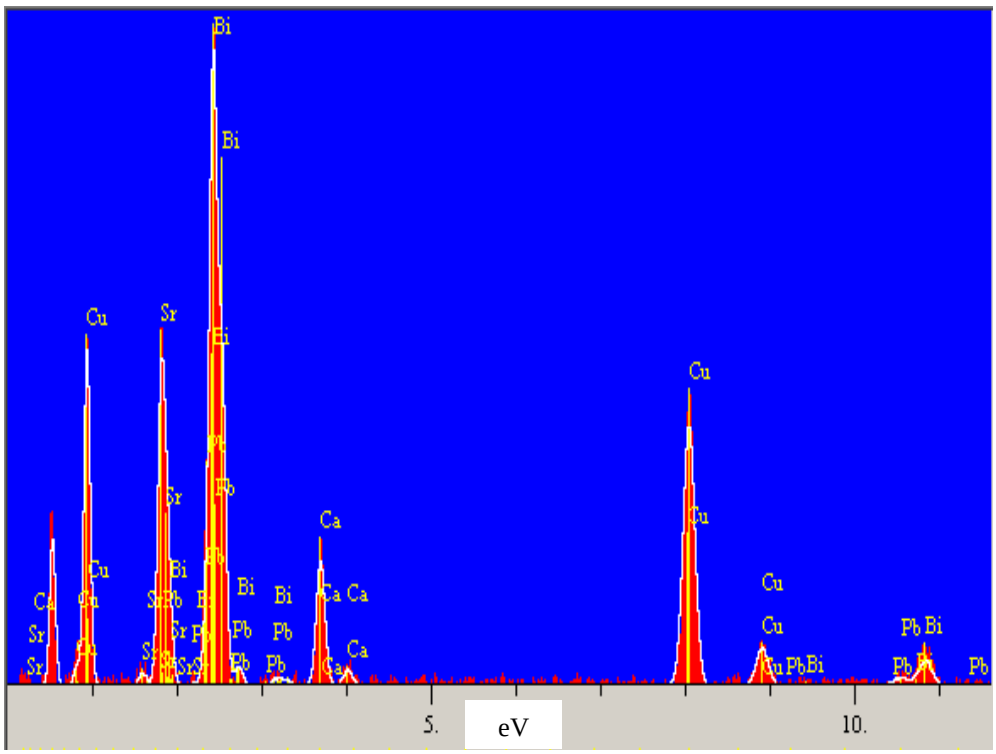

Figure 4.28: Energy dispersive spectrum analysis of Bi(Pb)SrCaCuO thin film fabricated at 850^0C for 2 hours.

Elt.	Line	Intensity (c/s)	Error 2-sig	EDS (Film)	Units	Target	Difference between target and results of EDS (%)
O	Ka	17.68	1.189	9.78	wt.%	13.73	-3.950
Ca	Ka	22.44	1.340	3.498	wt.%	5.50	-2.002
Cu	Ka	63.24	2.249	23.832	wt.%	12.00	+11.832
Sr	La	41.54	1.823	17.489	wt.%	15.05	+2.439
Pb	La	2.27	0.427	8.478	wt.%	17.79	-9.312
Bi	La	7.09	0.753	29.909	wt.%	35.90	-5.991
TOTAL				100.000	wt.%	100.00	

Table 4.9: Experimental and theoretical values of weight percent of $Bi_2Pb_1Sr_2Ca_{1.6}Cu_{2.2}O_8$ thin film fabricated at 850^0C for 2 hours.

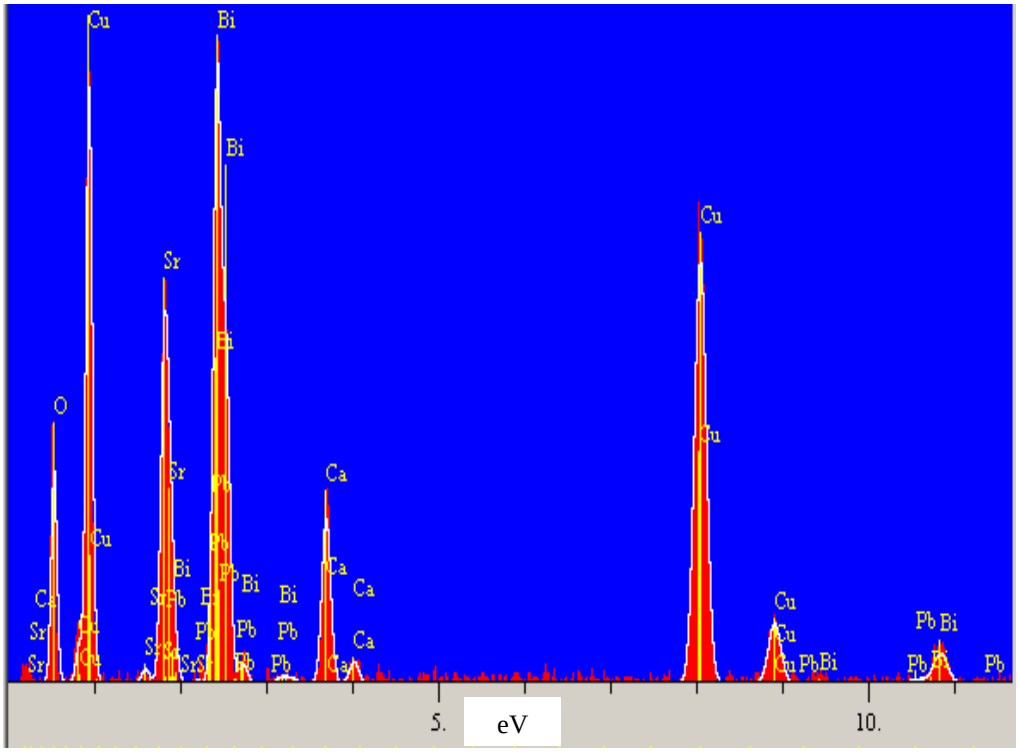

Figure 4.29: Energy dispersive spectrum analysis of Bi(Pb)SrCaCuO thin film fabricated at 850^0C for 4 hours.

Elt.	Line	Intensity (c/s)	Error 2-sig	EDS (Film)	Units	Target	Difference between target and results of EDS (%)
O	Ka	22.81	1.351	10.52	wt.%	13.73	-3.210
Ca	Ka	26.40	1.453	3.507	wt.%	5.50	-1.993
Cu	Ka	91.51	2.706	30.169	wt.%	12.00	+18.169
Sr	La	42.27	1.839	16.010	wt.%	15.05	+0.960
Pb	La	1.01	0.284	3.317	wt.%	17.79	-14.473
Bi	La	7.76	0.788	28.941	wt.%	35.90	-6.959
TOTAL				100.000	wt.%	100.00	

Table 4.10: Experimental and theoretical values of weight percent of $Bi_2Pb_1Sr_2Ca_{1.6}Cu_{2.2}O_8$ thin film fabricated at 850^0C for 4 hours.

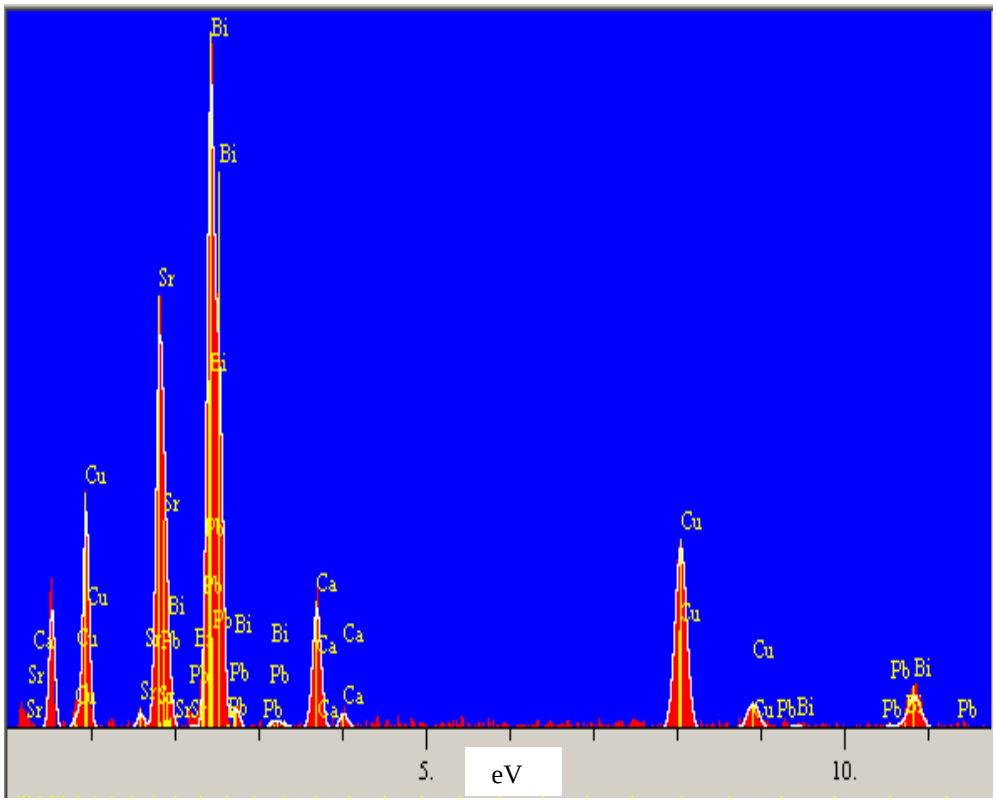

Figure 4.30: Energy dispersive spectrum analysis of Bi(Pb)SrCaCuO thin film fabricated at 850^0C for 6 hours.

Elt.	Line	Intensity (c/s)	Error 2-sig	EDS (Film)	Units	Target	Difference between target and results of EDS (%)
O	Ka	16.91	1.163	8.68	wt.%	13.73	-5.050
Ca	Ka	25.59	1.431	3.553	wt.%	5.50	-1.947
Cu	Ka	52.13	2.042	17.134	wt.%	12.00	+5.134
Sr	La	59.19	2.176	21.074	wt.%	15.05	+6.024
Pb	La	0.80	0.253	2.570	wt.%	17.79	-15.220
Bi	La	11.22	0.947	40.756	wt.%	35.90	+4.856
TOTAL				100.000	wt.%	100.00	

Table 4.11: Experimental and theoretical values of weight percent of $Bi_2Pb_1Sr_2Ca_{1.6}Cu_{2.2}O_8$ thin film fabricated at 850^0C for 6 hours.

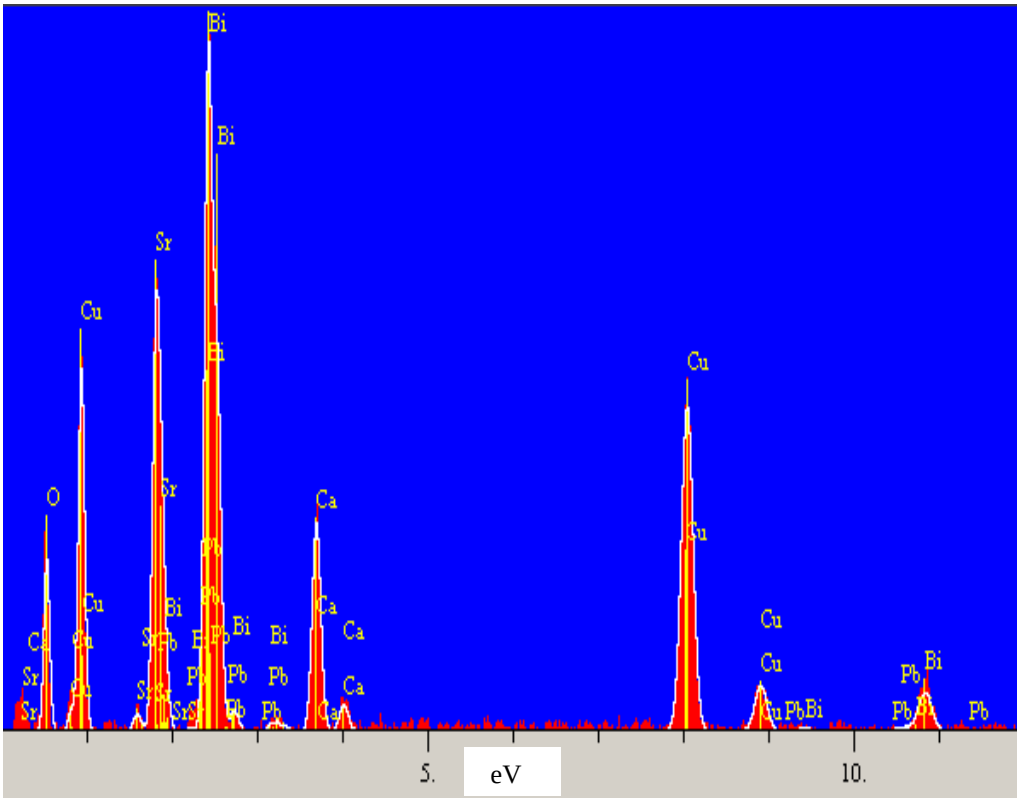

Figure 4.31: Energy dispersive spectrum analysis of Bi(Pb)SrCaCuO thin film fabricated at 850^0C for 8 hours.

Elt.	Line	Intensity (c/s)	Error 2-sig	EDS (Film)	Units	Target	Difference between target and results of EDS (%)
O	Ka	18.41	1.214	9.05	wt.%	13.73	-4.680
Ca	Ka	33.37	1.634	4.476	wt.%	5.50	-1.024
Cu	Ka	70.29	2.371	22.774	wt.%	12.00	+10.774
Sr	La	49.94	1.999	17.964	wt.%	15.05	+2.914
Pb	La	0.99	0.281	3.148	wt.%	17.79	-14.642
Bi	La	9.99	0.894	36.105	wt.%	35.90	+0.205
TOTAL				100.000	wt.%	100.00	

Table 4.12: Experimental and theoretical values of weight percent of $Bi_2Pb_1Sr_2Ca_{1.6}Cu_{2.2}O_8$ thin film fabricated at 850^0C for 8 hours.

Annealing Time and Temperature	Experimental Stoichiometric Ratios of Produced Films
1 hour-840^{0}C	$Bi_{1.70}Pb_{0.58}Sr_{2.76}Ca_{2.31}Cu_{2.38}O_{10.02}$
2 hours-840^{0}C	$Bi_{1.62}Pb_{0.60}Sr_{2.80}Ca_{2.30}Cu_{2.50}O_{10.19}$
4 hours-840^{0}C	$Bi_{1.74}Pb_{0.85}Sr_{2.55}Ca_{2.28}Cu_{1.87}O_{9.53}$
6 hours-840^{0}C	$Bi_{1.51}Pb_{0.14}Sr_{2.29}Ca_{1.98}Cu_{4.82}O_{11.55}$
8 hours-840^{0}C	$Bi_{2.60}Pb_{0.33}Sr_{2.57}Ca_{1.21}Cu_{1.89}O_{7.80}$
1 hour-850^{0}C	$Bi_{1.95}Pb_{0.29}Sr_{2.96}Ca_{1.18}Cu_{3.37}O_{8.68}$
2 hours-850^{0}C	$Bi_{1.66}Pb_{0.47}Sr_{2.32}Ca_{1.01}Cu_{4.36}O_{9.78}$
4 hours-850^{0}C	$Bi_{1.61}Pb_{0.18}Sr_{2.12}Ca_{1.02}Cu_{5.53}O_{10.52}$
6 hours-850^{0}C	$Bi_{2.27}Pb_{0.14}Sr_{2.80}Ca_{1.03}Cu_{3.14}O_{8.68}$
8 hours-850^{0}C	$Bi_{2.01}Pb_{0.17}Sr_{2.38}Ca_{1.30}Cu_{4.17}O_{9.05}$

Table 4.13: Calculated experimental stoichiometric ratios of produced films from target of $Bi_2Pb_1Sr_2Ca_{1.6}Cu_{2.2}O_8$

CHAPTER 5

CONCLUSION

In this thesis, we investigated the effects of different annealing times on T_c of $Bi_2Pb_1Sr_2Ca_{1.6}Cu_{2.2}O_8$ thin film samples annealed at 840^0C and 850^0C. XRD patterns, surface morphology (SEM), energy dispersive spectrum analysis (EDS), critical temperature, and resistivity measurements were examined. Among the films annealed at 840^0C, the highest critical temperature was obtained to be about 81 K for the film annealed for 8 hours. However, for the films annealed at 850^0C, the film annealed for 1 hour was found to have the highest critical temperature with 75 K. Moreover, resistivity dependence of temperature measurements for only the film annealed at 840^0C for 2 hours were carried out under field strengths of 0, 0.5, 1, 3 and 5 T, which were parallel and perpendicular to the film surface. It was seen that the T_c decreased with increasing the strength of the applied magnetic field. Furthermore, it was observed that the field applied to perpendicular to the film surface was more effective then the field applied to the parallel to the film surface. Volume fractions of Bi-2223 and Bi-2212 phases were also calculated for from XRD graphes. It was found that the T_c increases with the increase in the Bi-2223 volume fraction. Hence, the 8 hours annealing time at 840^0C was noted to be suitable to obtain the highest Bi-2223 volume fraction. In addition, according to the SEM results, flake-like and needle-like grains were observed in all samples; however, the film annealed for 8 hours at 840^0C was observed to obtain the denser grain than the others. Based on the results, in order to obtain the Bi-2223 volume fraction, the annealing time at 840^0C should be increased (or the annealing temperature at short time should be increased). In

other words, the annealing temperature at short time; or the more annealing time at 840^0C the more critical temperature we will obtain.

REFERENCES

[1] V. L. Ginzburg, E. A. Andryushin, Superconductivity, World Scientific Inc., USA (2004)

[2] M. Cyrot, D. Pavuna, Introduction to Superconductivity and High T_c Materials, World Scientific Inc., Singapore (1992).

[3] M. Tinkham, Introduction to Superconductivity, McGraw-Hill Inc., USA (1996).

[4] Thomas P. Sheahen, High Temperature Superconductors, Kluwer Academic Inc., USA (2002).

[5] Arcroft N.W., Mermin N.D., Solid State Physics, Harcourt Inc., Orlando (1976).

[6] A.C. Rose-Innes and E.H. Rhoderic, Introduction to Superconductivity, Pergamon Press, Great Britain (1978).

[7] Ajay Kumar Saxena, Springer Series in Materials Science High Temperature Superconductors, Springer Inc., Berlin, Heidelberg (2010).

[8] C. Michel, Superconductivity in Bi-Sr-Ca-Cu-O System, Zeitschrift für Physik B Condensed Matter, 68, (1987), 421-423.

[9] H. Maeda, Y. Taraka, Measurement of the Normal State Anisotropic Resistivity of Single Crystal Bi-Sr-Ca-Cu-O, Japanese Journal of Applied Physics, 27, 2 (1988), L209-L211.

[10] K. Tokano, Properties of Pb-Doped Bi-Sr-Ca-Cu-O Superconductors, Applied Physics Letters, 53,14, (1988), 1329-1331.

[11] J.B. Torrance, Y. Tokura, S. Laplaca, T.C. Huang, R.J. Savoy, A.I. Nazzal, New Class Of High - T_c Structures - Intergrowth Of Multiple Copper - Oxide Perovskite Like Layers With Double Sheets Of Bio, Solide State Communications, 66, (1988), 703-706.

[12] A. Kiliç, Master Thesis, University of Ankara, (2000).

[13] S. Koyama et al., Preparation of single 110 K phase of the Bi-Pb-Sr-Ca-Cu-O superconductor, Japanese Journal of Applied Physics, 27, (1988), L1861-L1863.

[14] R. Behrisch, Sputtering by Particle bombardment, Springer Inc., Berlin (1981).

[15] A. Varilci, M. Altunbas, O. Gorur, I. Karaca, and S. Celebi, Production of BiPbSrCaCuO Thin Films on MgO and Ag/MgO Substrates by Electron Beam Deposition Techniques, Physica Status Solidi (a) 194, No. 1, (2002), 206–215.

[16] C. Terzioglu, O. Ozturk, I. Belenli, The effect of Au diffusion on some physical properties of $Bi_{1.8}Pb_{0.35}Sr_{1.9}Ca_{2.1}Cu_3O_y$ superconductors, Journal of Alloys and Compounds, 471 (2009) 142–146.

[17] M. Akdogan, C. Terzioglu, A. Varilci, I. Belenli, Diffusion coefficient, activation energy and the effect of Ag-doping on some physical properties of silver doped $Bi_{1.8}Pb_{0.4}Ca_{2.2}Sr_2Cu_3O_x$, Physica B, 405 (2010) 4010–4019.

[18] C. W. Chiu, R. L. Meng, L. Gao, Z. J. Huang, F. Chen And Y. Y. Xue, Nature, 365, (1993), 323.

[19] S. A. Halim, S. A. Khawaldeh, S. B. Mohammed, H. Azhan, Superconducting properties of $Bi_{2-x}Pb_xSr_2Ca_2Cu_3O_y$ system derived via sol-gel and solid state routes, Materials Chemistry and Physics**,** 61, (1999), 251.

[20] K. Takasea, T. Shimizua, K. Makiharaa, H. Satob, H. Negishic, Y. Takahashia, Y. Takanoa, K. Sekizawaa, Y. Kuroiwad, S. Aoyagid, A. Utsumid,

A. Wadab, A. Inoe, H. Namatamee, M. Taniguchib, Electrical resistivity and photoemission spectra of layered oxysulfide ($La_{1-x}C_xO$)$Cu_{1-x}Ni_xS$, Physica B 329–333 (2003) 898–899.

[21] O. Oztürk, Ph-D Thesis, Abant İzzet Baysal University (2007).

[22] G. Yıldırım, M. Akdoğan, S. P. Altıntaş, M. Erdem, C. Terzioğlu, A. Varilci, Investigation of the magnetic field angle dependence of resistance, irreversibility field, upper critical field and critical current density in DC sputtered Bi-2223 thin film, Physica B 406 (2011) 1853-1857.

[23] R. J. Soulen Jr., S. A. Wolf, Magnetic phase diagrams for high transition temperature superconductors, Physica C: Superconductivity, 1-2, 166 (1990) 95.

[24] C. Terzioglu, H. Aydin, O. Ozturk, E. Bekiroglu, I. Belenli, The influence of Gd addition on microstructure and transport properties of Bi-2223, Physica B 403 (2008) 3354– 3359.

[25] H. Abbasi, J. Taghipour, H. Sedghi, Superconducting and transport properties of (Bi–Pb)–Sr–Ca–Cu–O with Cr_2O_3 additions, Journal of Alloys and Compounds 494 (2010) 305–308.

[26] C. Kittel, Introduction to Solid-State Physics, John Wiley and Sons, Inc., New York, London, Sydney (1986).